Geol. Mag. **152** (*5*), *2015, pp. 902–922.* © *Cambridge University Press 2015*
doi:10.1017/S0016756814000831

Sedimentary facies analyses from nano- to millimetre scale exploring past microbial activity in a high-altitude lake (Lake Son Kul, Central Asia)

MURIEL PACTON‡†*, PHILIPPE SORREL‡†*, BENOÎT BEVILLARD‡, AXELLE ZACAÏ‡, ARNAULD VINÇON-LAUGIER‡ & HEDI OBERHÄNSLI§¶

‡Laboratoire de Géologie de Lyon: Terre, Planètes, Environnement (UMR 5276 CNRS), Université Claude Bernard–Lyon 1, Villeurbanne, France
§Helmholtz-Centre Potsdam, German Geoscience Research Centre (GFZ), Section 5.2, Telegrafenberg, D-14473 Potsdam, Germany
¶Museum für Naturkunde, Leibnitz-Institute Berlin (Mineralogy), Invalidenstrasse 43, 10115 Berlin, Germany

(*Received* 28 July 2014; *accepted* 15 December 2014; *first published online* 2 March 2015)

Abstract – The fabric of sedimentary rocks in lacustrine archives usually contains long and continuous proxy records of biological, chemical and physical parameters that can be used to study past environmental and climatic variability. Here we propose an innovative approach to sedimentary facies analysis based on a coupled geomicrobiological and sedimentological study using high-resolution microscopic techniques in combination with mineralogical analyses. We test the applicability of this approach on Lake Son Kul, a high alpine lake in central Tien Shan (Kyrgyzstan) by looking at the mineral fabric and microbial communities observed down to the nanoscale. The characterization of microbe–mineral interactions allows the origin of four carbonate minerals (e.g. aragonite, dolomite, Mg-calcite, calcite) to be determined as primary or diagenetic phases in Lake Son Kul. Aragonite was mainly of primary origin and is driven by biological activity in the epilimnion, whereas diagenetic minerals such as Mg-calcite, calcite, dolomite and pyrite were triggered by bacterial sulphate reduction and possibly by methanotrophic archaea. A new morphotype of aragonite (i.e. spherulite-like precursor) occurs in Unit IV (c. 7100–5000 cal. BP) associated with microbial mat structures. The latter enhanced the preservation of viral relics, which have not yet been reported in Holocene lacustrine sediments. This study advocates that microbe–mineral interactions screened down to the nanoscale (e.g. virus-like particles) can be used successfully for a comprehensive description of the fabric of laminated lake sediments. In this sense, they complement traditional facies sedimentology tools and offer valuable new insights into: (1) the study of microbial and viral biosignatures in Quaternary sediments; and (2) palaeoenvironmental reconstructions.

Keywords: Facies sedimentology, geomicrobiology, organomineralization, virus-like particles, extracellular polymeric substances (EPS), high-altitude lake.

1. Introduction

Microfacies analysis commonly aims to determine the origin and distribution patterns of carbonate grains and the dominant biological control on carbonate sedimentation (Flügel, 2004). In addition to cathodoluminescence microscopy, fluid inclusion microscopy, scanning electron microscopy as well as stable isotope chemistry and X-ray techniques, facies analysis has become one of the common tools in sedimentological studies applied in marine settings (e.g. Flügel, 2004). In laminated lake sediments, it is increasingly used for the interpretation of seasonal palaeoclimate signals – including the rate, magnitude and direction of natural changes – as well as human impact on past environments by combining microscopical investigations with high-resolution X-ray fluorescence scanning analyses (e.g. Brauer *et al.* 2007; Sorrel *et al.* 2007; Neugebauer *et al.* 2012; Francus *et al.* 2013; Swierczynski *et al.* 2013). However, the characterization of microfacies (e.g. the fabric of sediments in laminated archives), including the biological contribution using electron and confocal microscopy, remains particularly poorly documented in lacustrine (palaeo)ecosystems. Past biological activity in lake sediments can be recorded as organic matter (OM) content, whose preservation is favoured under dysoxic to anoxic conditions, and fossil biosignatures. The OM content may reflect the water supply to the lake (Turcq *et al.* 2002) but is basically derived from both terrigenous inputs and autochthonous production in the lake. It is therefore of crucial importance to characterize the OM origin in order to decipher runoff and productivity related environmental changes (Prasad *et al.* 2007). This is usually achieved through comprehensive palynofacies analyses, although studying only OM does not allow microbe–mineral interactions to be deciphered.

†Authors for correspondence: muriel.pacton@univ-lyon1.fr, philippe.sorrel@univ-lyon1.fr
*These authors contributed equally to this work

Interest in the geomicrobiological approach has grown during the last decade as it has demonstrated the importance of linking geological and microbiological processes in palaeoenvironmental reconstructions. Organo-mineral interactions can be recorded in the geological record as microbial biosignatures. They include: (1) morphologically preserved microfossils; (2) stromatolite-like structures; (3) biologically induced or influenced minerals (e.g. Dupraz *et al.* 2009); and (4) organic chemical biomarkers (i.e. isotopic ratios, lipid biomarkers). In the absence of clearly identifiable remains of organisms, a variety of mineralogical biosignatures may infer past biological activity in an ecosystem (Banfield *et al.* 2001). Although authigenic minerals were previously used as palaeosalinity and palaeoproductivity proxies reflecting trophic state and/or early diagenetic conditions, they have also been considered as potential biosignatures of past microbial activity (Vuillemin *et al.* 2013).

This study investigates organic and mineral laminated sediments of alpine Lake Son Kul (Kyrgyzstan, Central Asia) using an innovative sedimentological and geomicrobiological approach which allows the recognition of morphological biosignatures. This includes a comprehensive and detailed characterization of the microfacies using: (1) microbial communities; (2) microbe–mineral interactions; and (3) mineral morphotypes. For that purpose we used high-resolution microscopy, which includes optical, scanning and transmission electron microscopy, in addition to confocal laser scanning microscopy, X-ray diffraction and X-ray fluorescence analyses of bulk sediments and extracted OM from palynological residues. This study will shed new light on the palaeoenvironmental conditions documented at Lake Son Kul during Holocene time (Huang *et al.* 2014; Lauterbach *et al.* 2014; Mathis *et al.* 2014), and provide new insights to further explore this complex alpine environmental system in central Tien Shan.

2. Geological and climate setting

Lake Son (= Son Kul or Kol) (41° 50′ 52″ N, 75° 07′ 45″ E, 3016 m asl) is a Kyrgyz alpine lake embedded in the central Tien Shan ranges (Fig. 1). It is the second-largest lake in Kyrgyzstan after Lake Issyk-Kul and also one of largest high-mountain lakes in the world. Today however, most inflow is contributed by groundwater (Beloglasova & Smirnova, 1987). The water column is well mixed and oxygenated down to the lake bottom in summer, as indicated by a site survey in July 2007. An oxygen minimum was found at a water depth of 1.5 m, reflecting ongoing respiration in the photic zone. Furthermore, according to earlier observations, H_2 and methane occurred near shores during the cold season. The high wind frequency controls the water mixing in the shallow lake. According to previous surveys, the weather is calm only during 11 % of the ice-free season (Beloglasova & Smirnova, 1987). This provides for a likely steady mixing of the water column and makes Lake Son Kul mostly a polymictic lake.

The annual mean air temperature is *c.* −3.5 °C, with summer temperature *c.* 11 °C and winter temperatures as low as −20 °C. Unlike Issyk-Kul, the Son Kul Lake water is fresh and is frozen between October and May.

3. Material and methods

3.a. Core sampling and chronology

In this study, we analysed a core retrieved during a field campaign in summer 2007. Piston core SK07 (1.52 m) was collected using a Usinger piston corer (http://www.uwitec.at) at Lake Son Kul (41° 46.196′ N, 75° 08.204′ E; water depth 12.5 m) (Fig. 2). Due to the coring procedure, the topmost 0.6 m is missing. The chronology of core SK07 is based on 11 AMS ^{14}C dates obtained on core SK07 and another core, SK04 (Mathis *et al.* 2014). Because the age model was already extensively discussed elsewhere (Huang *et al.* 2014; Mathis *et al.* 2014), we refer to those studies for a more comprehensive overview. The age model for core SK07 is depicted in Figure 2.

3.b. Mineralogy

For X-ray diffraction analyses (XRD) samples were ground to an ultrafine powder in an agate mortar. Organic-rich samples were treated by bleaching with a sodium hypochlorite solution. Samples were deposited on a plastic wafer in a plastic sample holder. We employed a Bruker AXS D8 Advance instrument, equipped with a linkeye counter and automatic sampler rotating the sample (ETH Zürich).

3.c. Facies analyses

For microfacies analyses and micro-XRF scanning, we prepared a series of 2.5-cm-long sediment samples from the interval 87–95 cm in core SK07 (Fig. 3). The samples were freeze-dried, soaked in a transparent epoxy resin (Araldite® 2020; Vantico, Basel, Switzerland) and subsequently polished at the University of Geneva (Switzerland). Thin-sections were analysed under parallel and polarized light with a microscope Leica DM750P (Germany). Magnifications used were 25× (overview), 40× and 100× (measurement of lamination thickness and microfacies description; error: 20 μm). Thin-section photographs were obtained using a digital camera Leica EC3 equipped with the Leica Acquire 1.0 software.

3.d. Electron microscopy

Bulk sediments and palynological residues (i.e. isolated OM) were studied using scanning electron microscopy (SEM) prior to fixation with glutaraldehyde and were subsequently platinum- or gold/palladium-coated,

https://doi.org/10.1017/S0016756814000831 Published online by Cambridge University Press

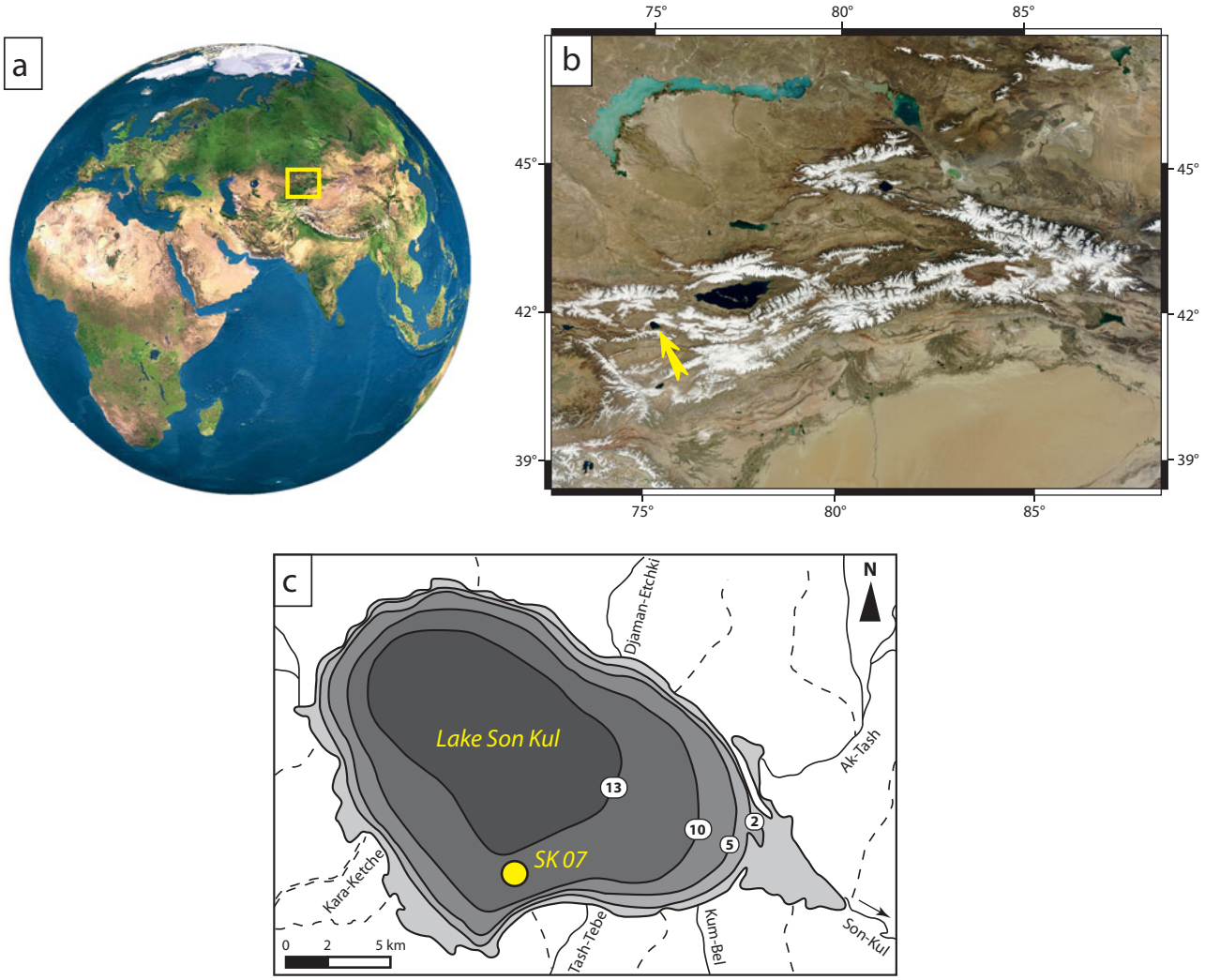

Figure 1. (Colour online) Location of Lake Son Kul: (a) global map with focus on western central Asia; (b) central Tien Shan including south Kazakhstan and Lake Balkash (image courtesy of NASA GSFC); and (c) bathymetric map of Son Kul basin with coring site SK07 in the southern part of the lake.

using a FEI Quanta 250 FEG at the Centre Technologique des Microstructures at the University Lyon 1 (France). Semi-quantitative elemental analyses of micron-sized spots were obtained using an EDAX energy-dispersive X-ray spectrometer (EDS Centre Technologique des Microstructures) during SEM observations. The OM ultrastructure from two selected samples (3.2–4 cm in Unit I and 88–90 cm in Unit IV) was subsequently investigated using transmission electron microscopy (TEM). For TEM observations, fossil OM was fixed in 1 % glutaraldehyde in 50 mM cacodylate buffer at pH 7.4 (CB) and at room temperature for one hour, washed three times in CB and post-fixed in 1 % osmium tetroxyde in CB for one hour at room temperature. After three washes in CB, the material was embedded in 2.5 % agarose and dehydrated before inclusion in Epon. Ultrathin sections (70 nm) were obtained using a Leica ultra-microtome and stained with lead citrate uranyl acetate for 15 min. TEM observations were performed with a Phillips CM100 transmission electron microscope (Centre Technologique des Microstructures, University Lyon 1) and digital image processing was applied.

3.e. Fluorescence *in situ* hybridization

The morphology and distribution of microbial species in core SK07 (Fig. 4) was examined by fluorescence *in situ* hybridization (FISH; e.g. Amann, Ludwig & Schleifer, 1995). This approach is based on the combination of oligonucleotide probes, which are specifically designed for identifying precise bacterial species or phyla. When these probes are labelled with fluorescent dyes, they can be used to identify single microbial cells directly by FISH. Twelve samples (1–4 cm long) were stained both with the 16S rRNA probe SRB385 (CGGCGTCGCTGCGTCAGG) labelled with cyanine 3 to image sulphate-reducing bacteria (SRB) and with the 16S rRNA probe ARCH915 (GTG CTC CCC CGC CAA TTC CT) labelled with FTIC to image archaea. The SRB385 oligoprobe targets SRB of the y-proteobacteria (Amann *et al.* 1990). Sediment samples

https://doi.org/10.1017/S0016756814000831 Published online by Cambridge University Press

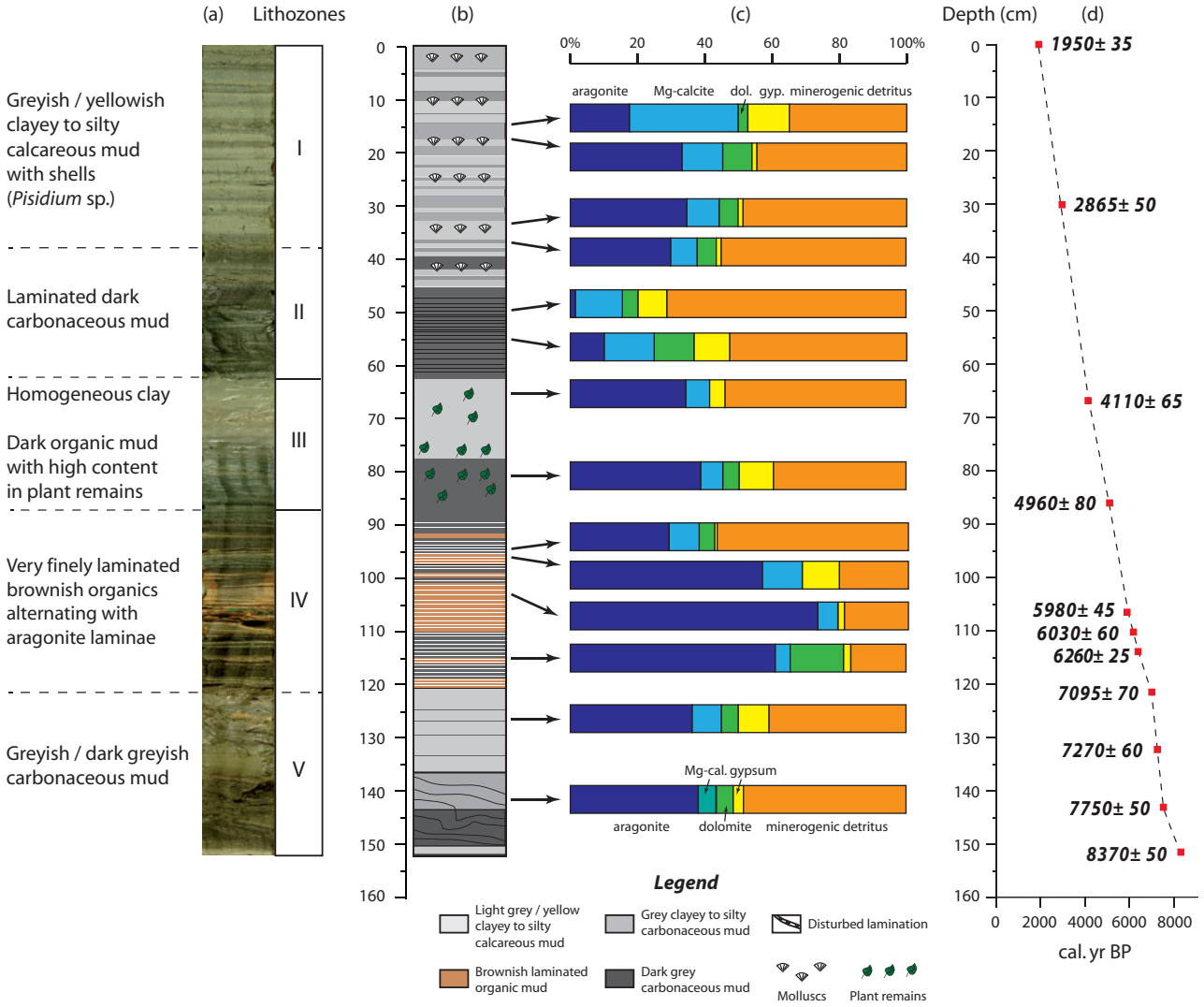

Figure 2. (Colour online) (a) Lithozones, (b) simplified lithology, (c) mineralogical data based on XRD analyses and (d) age model for Son Kul core SK07.

were first fixed with an aqueous solution containing 2 % (v/v) paraformaldehyde, air-dried on a glass slide and then dehydrated sequentially by ethanol solutions of 50, 80 and 96 % for 3 min each. The dehydrated sample was air-dried again, and hybridized with 1 μL each of the oligonucleotide probe solutions (100 ng mL^{-1}) and 10 mL of a formamide-containing hybridization buffer (0.9 M NaCl, 0.01 % SDS, 20 mM Tris-HCl, pH 7.2). Hybridization took place at 46 °C in a sealed moisture chamber for 90 min, followed by incubation in washing buffer (0.07 M NaCl, 0.01 % SDS, 20 mM Tris/HCl, 5 mM EDTA, pH 7.2) at 48 °C for 30 min. The glass slide was then rinsed with distilled water and air-dried before examination under a confocal laser scanning microscope (CLSM, Zeiss LSM 510 META).

3.f. Micro X-ray fluorescence

Major and trace element mapping were analysed by Micro X-ray fluorescence using an EAGLE III μ-probe spectrometer (μ-XRF; EDAX Inc., Mahwah, NJ, USA; faisceau 50 μm) at the University of Geneva (Switzerland).

4. Results

4.a. Sedimentary facies

Based on macro- and microfacies properties, texture, macrofossils, mineralogy (e.g. XRD analyses) and morphological biosignatures, we have subdivided core SK07 into five lithological units (I–V; Fig. 2) described in the following. Sediments from core SK07 contain authigenic minerals (aragonite, Mg-calcite, gypsum and dolomite) and detrital silicates (quartz, feldspars such as albite and clay minerals).

Unit I (0–38 cm; c. 3100–1950 cal. BP) is characterized by alternating greyish and yellowish clayey to silty calcareous muds forming 0.5–5-cm-thick beds. Ostracoda and diatoms are rather common in this unit, but mollusc shells remain confined to the greyish thick layers. Sediments from this unit are composed of about 40 % of detrital minerals (mainly albite, quartz and

https://doi.org/10.1017/S0016756814000831 Published online by Cambridge University Press

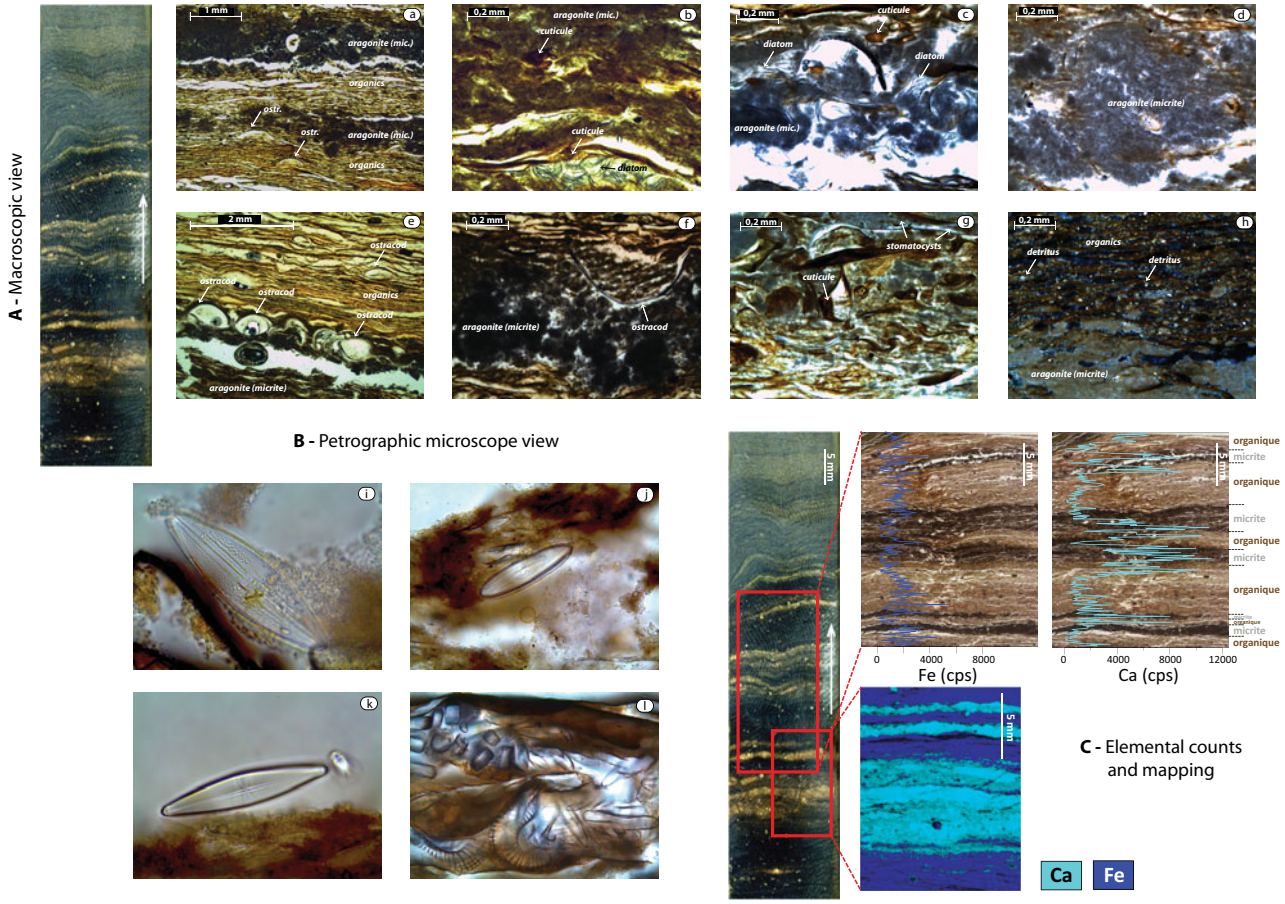

Figure 3. (Colour online) Thin sections (facies) images of the laminated interval in Unit III (cross polarized right). (A) Macroscopic view of the studied interval (87–95 cm) in core SK07. (B) Petrographic microscope view of (a–h) the fabric of laminated sediments with (i–l) diatom occurrences. (a) Alternating laminae of dense micrite showing fluffy patches of aragonite and organic matter including diatoms; (b–d) dense micrite lamina including plant cuticles (b) and diatoms (c); (e) sharp transition between micrite and organic matter laminae (note the enrichment in ostracods at the top of the micrite lamina); (f) close-up of dense micrite lamina showing fluffy patches of aragonite; (g) transition between micrite and organic matter laminae (note the enrichment in plant cuticles and sheet-like vegetal fragments at the top of the organic lamina and the presence of stomatocysts); and (h) close-up of transition between micrite and organic matter laminae (note the presence in minerogenic detritus in the organic lamina). (i) *Anomoneis cf. sphaerophora* (100× magnification); (j) *Caloneis spp*. (40× magnification); (k) *Gomphonema spp*. (100× magnification); and (l) diatom bloom including *Campylodiscus* spp. and *Caloneis* sp. (40× magnification), (C) μ-XRF measurements of selected chemical elements (Ca, Fe) on impregnated block used to make thin-sections. Upper: μ-XRF data show the enrichment of Ca (Fe) in the micrite (organic) laminae; lower panel: same pattern but as elemental map.

micas) and 50 % of carbonates as based on XRD analyses (Fig. 2). Light-coloured laminae are enriched in aragonite in contrast to the greyish laminae, while dolomite averages *c.* 9 % of the mineral matrix.

Unit II (38–63 cm; c. 4000–3100 cal. BP) is characterized by a pronounced lithology and colour change. Its laminations consist of interspersed dark and dark-grey calcareous mud layers. Ostracoda and diatoms are abundant in the greyish layers while mollusc shells are absent. Mineralogical analyses show that Unit II exhibits the lowest aragonite content (less than 5 %) for the entire core SK07, while the minerogenic detritus dominates this unit. Content of gypsum (up to 20 %) and Mg-calcite are relatively high, whereas dolomite abundance is about 5 %.

Unit III (63–87 cm; c. 5000–4000 cal. BP) consists of thick greyish calcareous clay layers. This unit displays aragonite and Mg-calcite contents similar to the light-coloured laminae from Unit I, while gypsum content is *c.* 4 %. It is worth noting that no dolomite was found in this unit.

Macroscopically, the very well-laminated *Unit IV* (87–122 cm; c. 7100–5000 cal. BP) consists of finely laminated yellowish calcareous mud interbedded with white aragonite and dark brown organic layers. Accordingly, observations under the petrographic microscope reveal two kinds of laminae (Fig. 3a). The first type of lamina is a dense micrite (e.g. aragonitic) lamina with traces of organic matter and very rare detrital grains (Fig. 3b–f). The laminae are enriched in ostracods (Fig. 3e) and diatoms, the latter occurring in the form of blooms in the matrix (Fig. 3c, l). Dominant and subdominant diatom taxa are *Anomoneis* cf. *sphaerophora*, *Gomphonema* spp., *Caloneis* spp., *Campylodiscus* spp., *Scoliotropis* spp., *Stauroneis* spp. and *Pinnularia* spp. (Fig. 3i–l). A few chrysophyte

https://doi.org/10.1017/S0016756814000831 Published online by Cambridge University Press

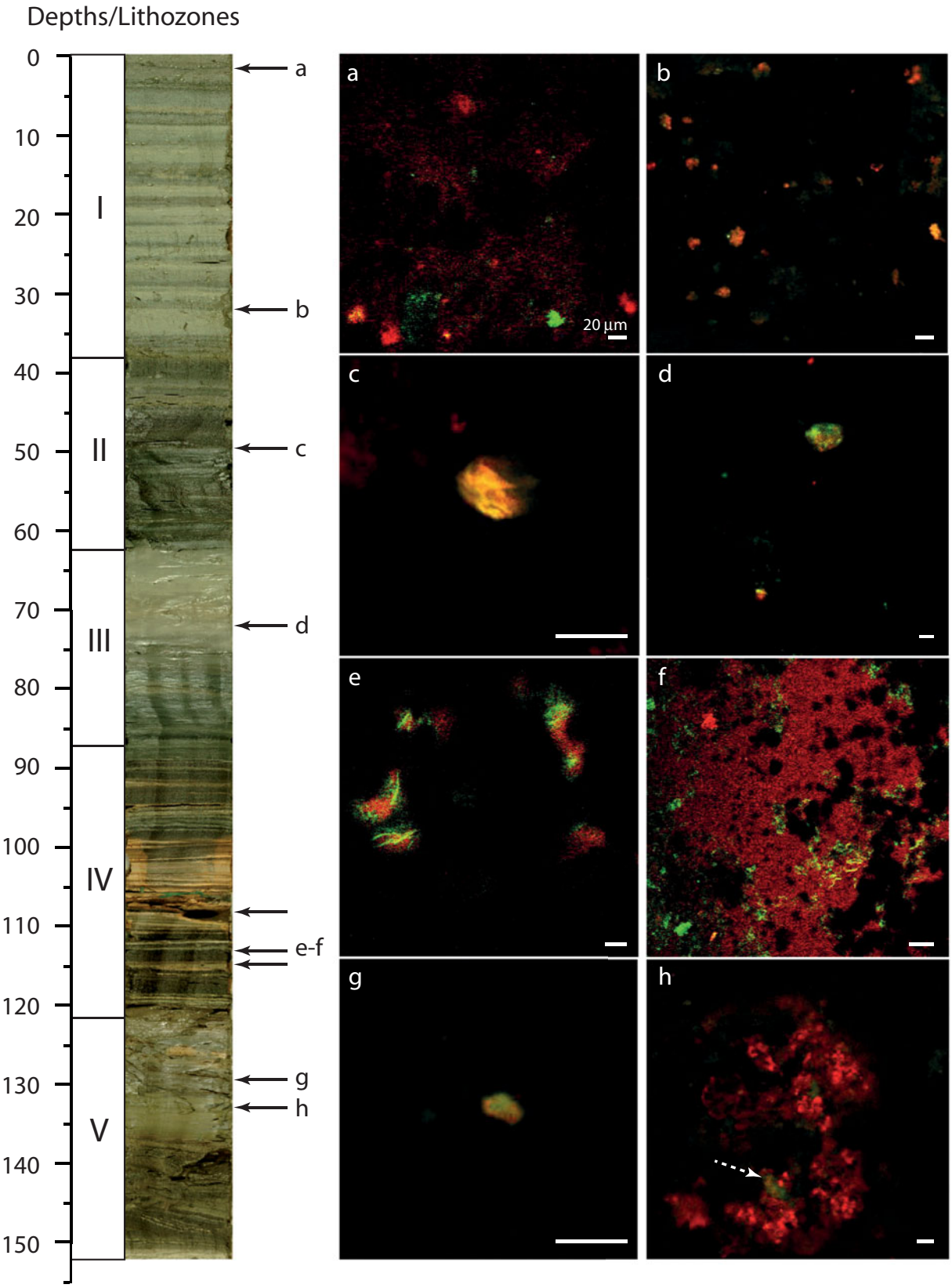

Figure 4. (Colour online) FISH analysis to localize specific SRB (artificial colour red) and archaea (artificial colour green) populations in sediments from Son Kul core SK07. Scale bars: 20 µm. All panels show confocal laser scanning micrographs. (a) Abundant SRB in dark layers of Unit I in surface sediments (1.5–2 cm depth). (b) Monospecific aggregates of archaea in the yellowish layers of Unit I (at 32 cm). Some aggregates exhibit a yellow fluorescence (arrow) where the SRB and archaea are completely mixed. (c) Syntrophic colony with bacteria intertwined with filamentous archaea in Unit II sediments (49.5–50 cm). (d) Isolated SRB aggregates in Unit III (72 cm). (e) Archaea/SRB consortia resulting in large aggregates in which archaea are tightly associated in monospecific clusters (Unit IV, 112.5–113.5 cm, dark brown organic lamina). (f) Large abundance of SRB over archaea (Unit IV, 112.5–113.5 cm interface between organic and micrite laminae). (g) Archaea and SRB are almost absent from the micrite laminae of Unit V (128–129 cm). (h) SRB aggregates observed in randomized patches from the dark greyish layers in Unit V (131.5–132 cm).

https://doi.org/10.1017/S0016756814000831 Published online by Cambridge University Press

stomatocysts are also encountered (Fig. 3g). Under the μ-XRF core scanner, these laminae are Ca rich (Fig. 3C). The second type of lamina, forming the dark brown macroscopic layers, mainly comprises organic matter. The lamina is composed of an organic matrix including angular very fine to medium (e.g. mineral silt and clay) detrital material (mainly quartz and micas), plant cuticles and undifferentiated vegetal fragments. Diatoms are less common in the thin-sections. Some laminae can be as thin as 70 μm in thickness. μ-XRF data show that these laminae are enriched in Fe but poor in Ca, revealing a clear opposite pattern (anti-correlation) between the two types of laminae. XRD analyses reveal that sediments from Unit IV display the highest content in aragonite in core SK07 (Fig. 2). Although the micrite laminae are dominated by aragonite (up to 74 %), they do not show a clear pattern in terms of mineral distribution for dolomite and gypsum when compared with the dark brown laminae. Gypsum seems to be more abundant in the upper part of Unit IV (between 87 and 100 cm), while dolomite exhibits the highest content at the base of Unit IV in micrite laminae (11 %). Note that no dolomite was found in the micrite laminae from the upper part of Unit IV. Mg-calcite is relatively low in this unit, regardless of the dark brown/micrite lamina distribution.

Unit V (122–152 cm; c. 8350–7100 cal. BP), with partly disturbed layering in the lowermost part of the core, consists again of greyish calcareous mud layers interbedded with dark greyish calcareous mud layers. Aragonite and detrital minerals predominantly characterize sediments from Unit V. Mg-calcite, dolomite and gypsum average 6 %, 5 % and 7 %, respectively. It is worth noting that sediments from the interval 120–135 cm are significantly enriched in gypsum (9 %). The disturbed layers at the bottom of the core may have suffered cryoturbation shortly after deposition.

4.b. Electron microscopy (SEM, TEM)

Under SEM, facies analyses in Unit I indicate the presence of slightly dissolved diatoms, biogenic siliceous microspheres named chrysophyte stomatocysts, framboidal pyrites and the chlorococcalean algae *Botryococcus braunii* and *Pediastrum sp*. trapped in the carbonaceous matrix (Fig. 5; supplementary Figs S1, 2, available at http://journals.cambridge.org/geo). The main discrepancies between the greyish and light-coloured layers are the presence of distinct aragonite rods in the yellowish layers and the predominance of gypsum in the greyish layers. Both laminae however contain extracellular polymeric substances (EPS) characterized by an alveolar network, which are closely associated with Mg-carbonates and the surrounding Mg–Al silicate matrix (supplementary Fig. S1). SEM investigations of OM reveal *B. braunii*, *Pediastrum sp.*, plant cuticles and framboidal pyrites in both types of laminae (Fig. 5; supplementary Figs S1, 2). Another difference between yellowish and greyish laminae resides in the preservation state of organic components, enhanced in greyish laminae (supplementary Fig. S2d), along with more abundant framboidal pyrites compared to the light-coloured laminae. Very rare euhedral pyrite was found in the yellowish laminae, showing dissolution features (supplementary Fig. S1f). In both types of laminae microbial signatures are abundant: tracheids are largely colonized by microbes (supplementary Fig. S2e) in the greyish layers, while *B. braunii* are slightly degraded by microbes as shown by abundant filamentous EPS leading to a fluffy aspect on algae surface. In the yellowish laminae, nanometre-scale spheroids in the size range 60–200 nm are frequently found embedded within EPS (Fig. 5e) and are referred to as virus-like particles (VLPs). Nanofilaments (less than 150 nm in diameter but extending several microns in length) are also encountered and resemble nanowires, which are closely associated with bacteria (Fig. 5f). Ultrastructure of OM in the yellowish laminae shows ultralaminae and fluffy EPS (Fig. 6a) along with plant cuticles, prokaryotic cells with intracellular inclusions (Fig. 6b) and abundant VLPs showing a typical hexagonal shape (Fig. 6c).

Unit II is made up of thick dark-greyish calcareous mud layers and contains abundant and well-preserved different diatom communities, chrysophyte stomatocysts, *B. braunii*, microbial filaments and framboidal pyrites (Fig. 7). Most stomatocysts are small, smooth and spherical (less than 5 μm in diameter) with a cylindrical collar (1.2 μm in diameter and 0.3 μm in height). They resemble Stomatocyst 52 as defined by Duff, Zeeb & Smol (1995). Microfossils are exceptionally well preserved as shown by intact diatom frustules and the presence of a cap still attached to the stomatocysts (Fig. 7e).

Unit III consists of homogeneous light-coloured greyish calcareous muds and reflects the dominance of aragonite rods and detrital particles such as clays (Fig. 8). This unit is characterized by the absence of diatoms, while *B. braunii* is rare. Microbial features are abundant and characterized as filamentous microorganisms, VLPs and EPS (Fig. 8b–e). The latter are closely associated with Mg-carbonate, showing a rhomboedral shape (Fig. 8e–f).

Unit IV mostly displays aragonite under SEM. Aragonite is principally in the form of rods (Fig. 9a), but stars are also present in both dark and white laminae (supplementary Fig. S3a, available at http://journals.cambridge.org/geo). Aggregates of carbonates, likely low Mg-calcite, contain small amounts of Si (supplementary Fig. S3b). These aggregates are surrounded by EPS showing an aluminosilicate composition plus Mg. At a higher magnification, EPS embed detrital minerals, aragonite and other Mg-carbonates and seem to create a matrix leading to the preservation of VLPs (Fig. 9b). Examinations of OM under SEM show distinct aspects depending on the types of laminae. Dark brown organic laminae show abundant figured OM such as *B. braunii* and plant cuticles, which are extensively colonized and

https://doi.org/10.1017/S0016756814000831 Published online by Cambridge University Press

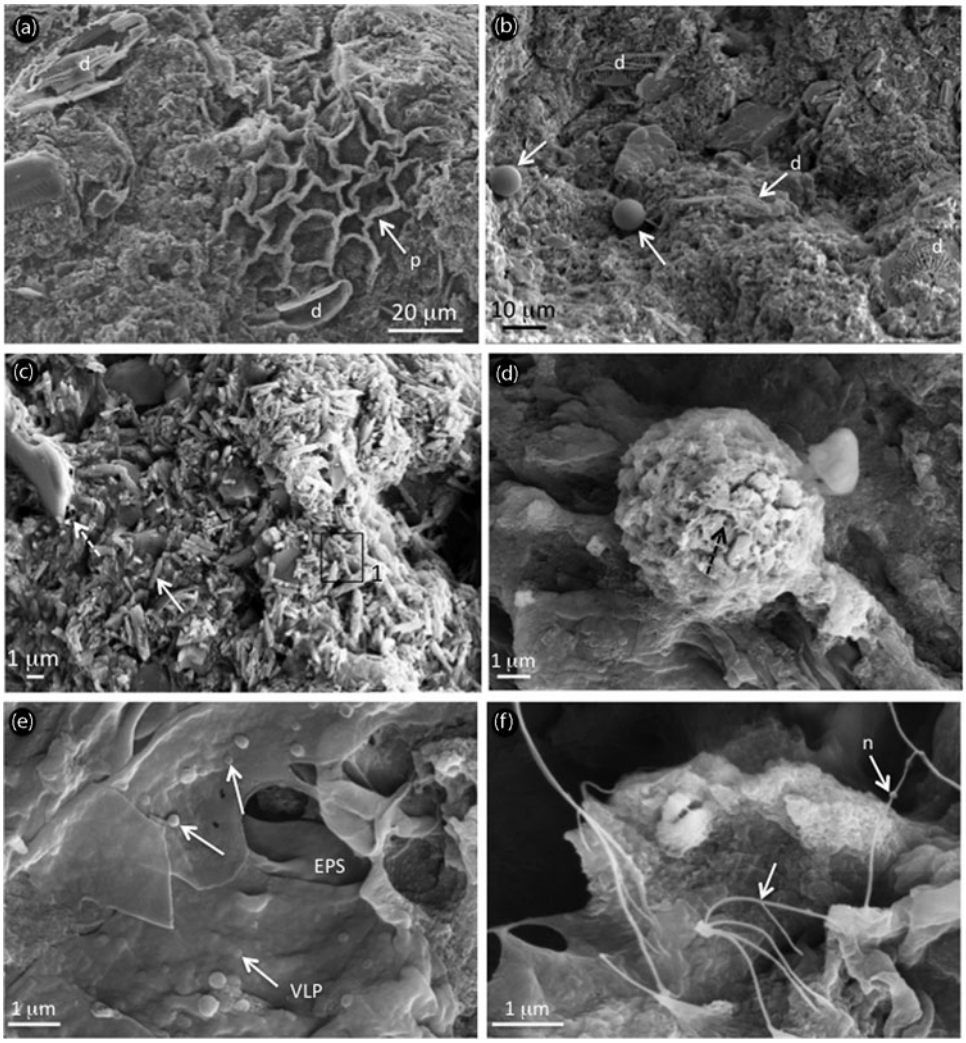

Figure 5. SEM photomicrographs and associated elemental analyses showing (a–d) microfossils and microstructure of precipitates and (d–f) organic matter after acid etching from Unit I in the light-coloured layer. (a) Intact to slightly dissolved diatoms ('d') and *Pediastrum sp*. ('p') trapped in the carbonate mud; (b) different diatom populations ('d') and chrysophytes (white arrows); (c) aragonite as rods (white arrow), embedded in a matrix containing EPS alveolar structure (dashed arrow); (d) partially dissolved framboidal pyrite as shown by numerous holes (dashed arrow); (e) virus-like particles ('VLP', arrows) embedded within EPS; and (f) nanowires ('n', arrows).

degraded by microbes as shown by the wide abundance of EPS (Fig. 9c). Isolated coccoid prokaryotes were found within EPS, but only one pyrite crystal was found in this unit within the organic laminae (supplementary Fig. S3c). Conversely, as well as the colonization of figured OM by microbes (supplementary Fig. S3d, e), the aragonite laminae contain abundant colonies of coccoid prokaryotes closely associated with EPS which seem to be independent of figured OM (Fig. 9d, e; supplementary S3e–f). Abundant VLPs have been found on prokaryote surfaces (Fig. 9d, f). Ultrastructure of OM from both aragonite and organic laminae (88–90 cm depth) reveals ultralaminae (Fig. 6d) and different prokaryotic cells, such as microbial cells with intracellular cytoplasmic membrane resembling thylakoids (Fig. 6d). EPS were distributed as either a fluffy network (Fig. 6f) or condensed alveolar network with holes of different orders of magnitude (Fig. 6e). VLPs are characterized by a hexagonal shape (capsid-like), sometimes with a tail attached to it (Fig. 6f).

Unit V is divided in two intervals: (1) greyish calcareous mud layers, interbedded with (2) dark greyish calcareous mud layers. The uppermost interval is dominated by aragonite as rods and stars (Fig. 10a). Other mineral phases have been found such as low Mg-calcite, which occurs as rhomboedra containing minor Si (Fig. 10b; supplementary Fig. S4a, available at http://journals.cambridge.org/geo) and other Mg-carbonate aggregates (Fig. 10c). Aragonite crystals are embedded within an aluminosilicate matrix resembling EPS, which contains mainly Mg and Si (Fig. 10b; supplementary Fig. S4a, b). EPS are widely distributed and can be clearly recognized as filaments (Fig. 10c; supplementary Fig. S4c). The lowermost interval displays well-crystallized aragonite stars (Fig. 10d) and rods (Fig. 10e; supplementary Fig. S4d). Mg-carbonates containing Si were found as nanometre-size rhombs,

https://doi.org/10.1017/S0016756814000831 Published online by Cambridge University Press

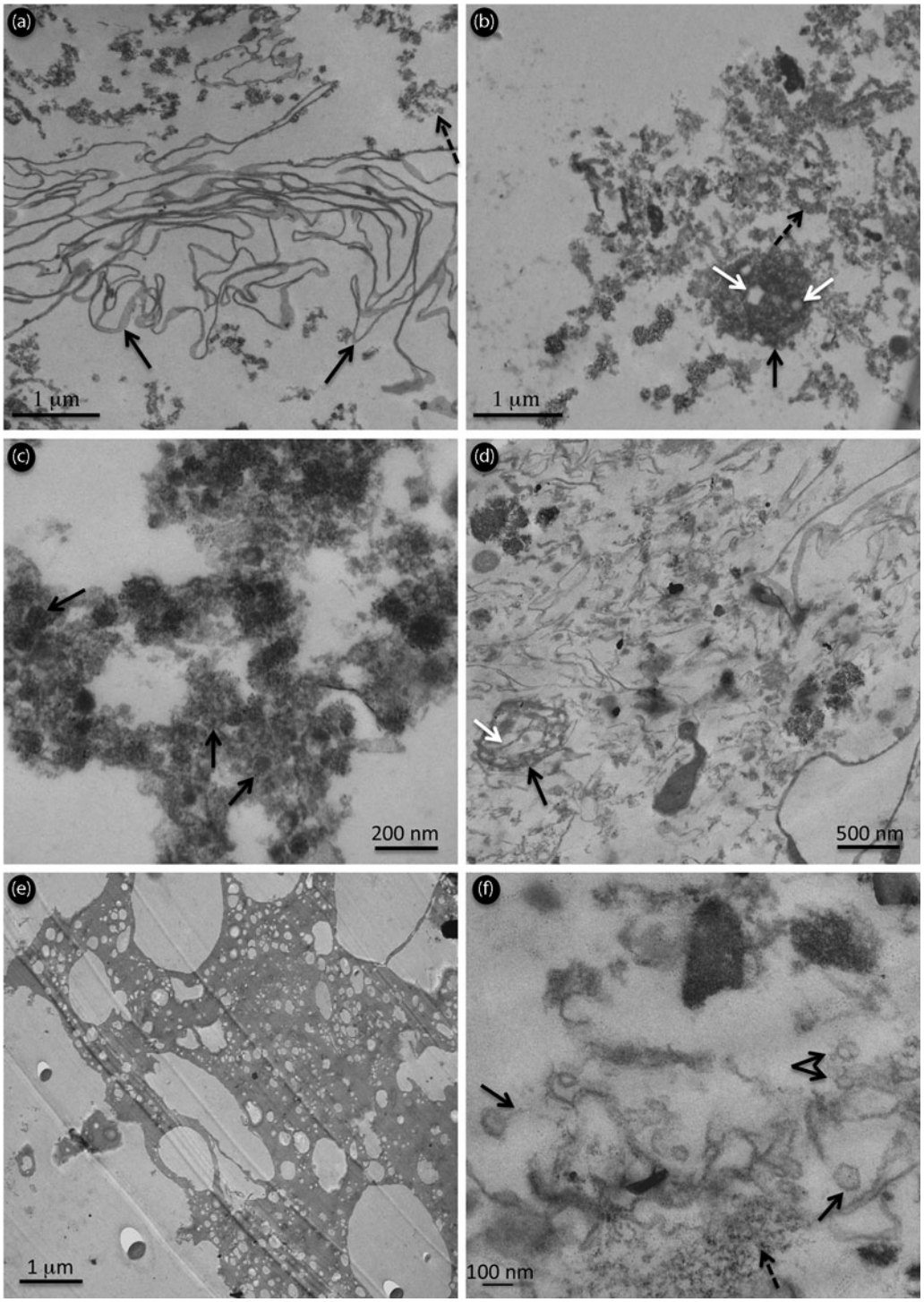

Figure 6. TEM sections of organic matter after acid etching from (a–c) Unit I in the greyish layer (3.2–4 cm) and (d–f) Unit IV in the dark greyish layer (88–90 cm) showing: (a) ultralaminae as bacterial cell walls (arrows) and EPS (dashed arrows); (b) bacterial cell (black arrow) containing different intracellular inclusions (white arrows) and bacterial cell walls (dashed arrow); (c) virus-like particles (VLP; arrows); (d) small cyanobacterium (black arrow) containing thylakoid membranes (white arrows); (e) EPS characterized by an alveolar network; and (f) VLP characterized by an icosahedral shape (black arrows) and sometimes a tail and fluffy EPS (dashed arrow).

which are closely associated with EPS (Fig. 10e). Some diatoms were also identified (Fig. 10d). Microbial features are well preserved and widely distributed as EPS in the form of filaments (Fig. 10e; supplementary Fig. S4f) and of stretched-out veils (Fig. 10f; supplementary Fig. S4f). The latter are surrounding Mg-carbonate crystals (Fig. 10f).

4.c. Fluorescence *in situ* hybridization

The SRB and archaea populations in the sediments were determined based on FISH images using specific probe combinations. Figure 4 illustrates the FISH image using the Archaea-specific probe ARCH915 and the SRB-specific probe SRB385.

https://doi.org/10.1017/S0016756814000831 Published online by Cambridge University Press

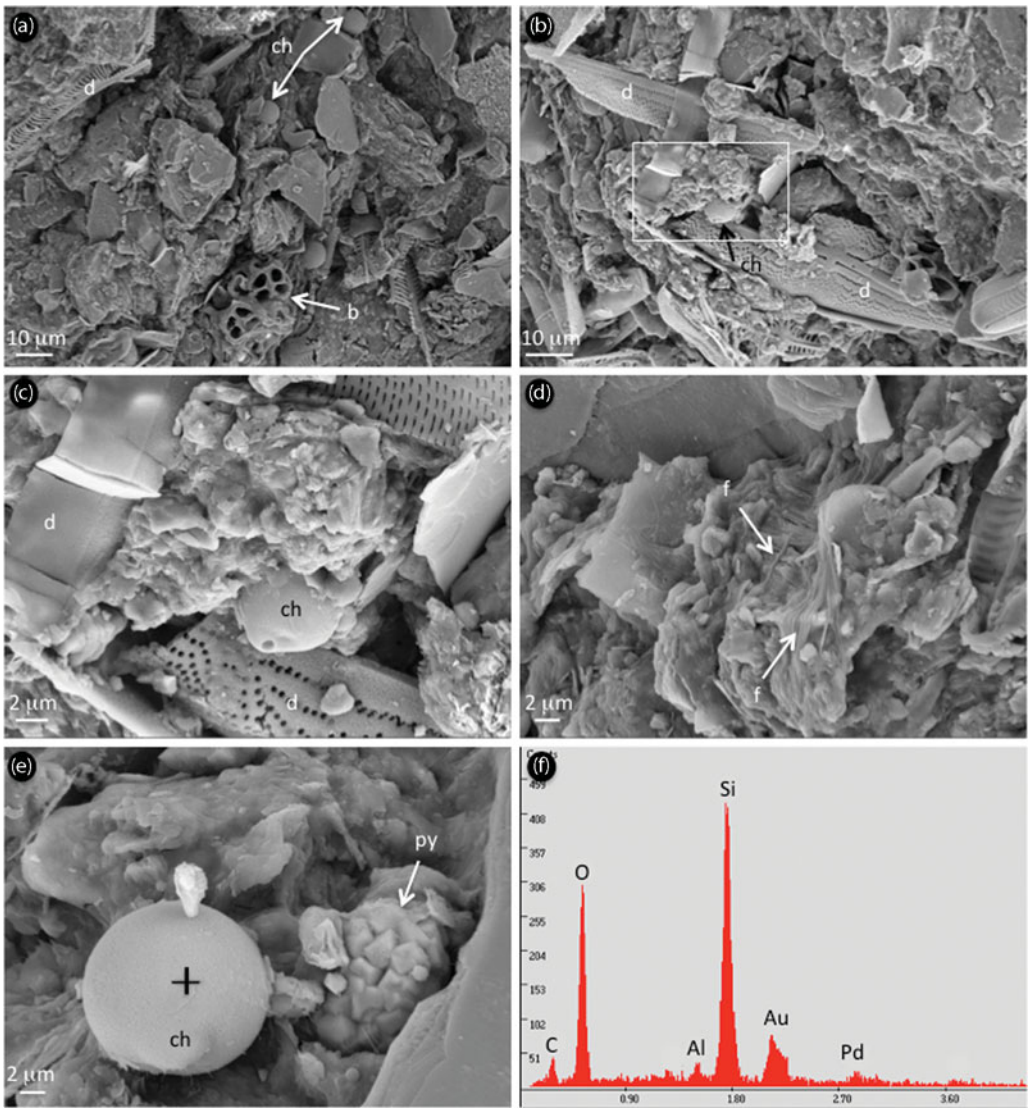

Figure 7. (Colour online) SEM photomicrographs showing microfossils and microstructure of precipitates from Unit II: (a) slightly dissolved diatoms ('d'), *Botryococcus braunii* ('b') and chrysophytes ('ch'); (b, c) well-preserved diatom frustules ('d'); (d) filamentous microbes ('f'); (e) framboidal pyrite (white arrow) and chrysophyte ('ch') with the cap still preserved and attached in the pore; and (f) elemental analysis of the chrysophyte confirming the Si cyst.

FISH surveys of microbial cells in 12 samples revealed a qualitative variable abundance and distribution of SRB and archaea (Fig. 4). Unit I is characterized by an abundance of SRB over archaea in the yellowish laminae (Fig. 4a), while SRB and archaea coexist together in aggregates in the greyish laminae (Fig. 4b). Few microbes were found in Units II and III, but both SRB and archaea occur together in aggregates (Fig. 4c, d) and were sometimes even mixed (Fig. 4c). Unit IV showed distinct patterns of microbial distribution. In the dark brown organic layers archaea/SRB consortia were abundant and resulted in either large aggregates in which archaea are closely associated in monospecific clusters (Fig. 4e), or in SRB prevailing over archaea at the interface between organic and micrite laminae (Fig. 4f). Few microbes were found in the aragonite layers and archaea and SRB occurred as a consortium in aggregates (Fig. 4g) in Unit V. Dark greyish layers are characterized by an abundance of SRB over archaea (Fig. 4h).

5. Interpretation and discussion

5.a. Microbial biosignatures

5.a.1. Microbial processes

Palynological analysis of Son Kul sediments reveals an important contribution of amorphous OM (Mathis *et al.* 2014). This amorphous OM is of granular aspect, suggesting a microbial origin (Pacton, Gorin & Vasconcelos, 2011). This is in agreement with the wide abundance of filamentous and coccoid microbes along with EPS found in the different units (e.g. Figs 5–10). EPS are usually found as isolated nanofilaments associated with Mg-carbonates or as fluffy particles in palynological residues (with evidences of degradation of figured particles) from all units except Unit IV. In these units, the local occurrence of nanofilaments of EPS along with the numerous bacterial cell walls observed in Unit I, referred to as ultralaminae (see Pacton, Fiet & Gorin, 2008 for a comprehensive review), support the hypothesis that OM is mainly derived from

https://doi.org/10.1017/S0016756814000831 Published online by Cambridge University Press

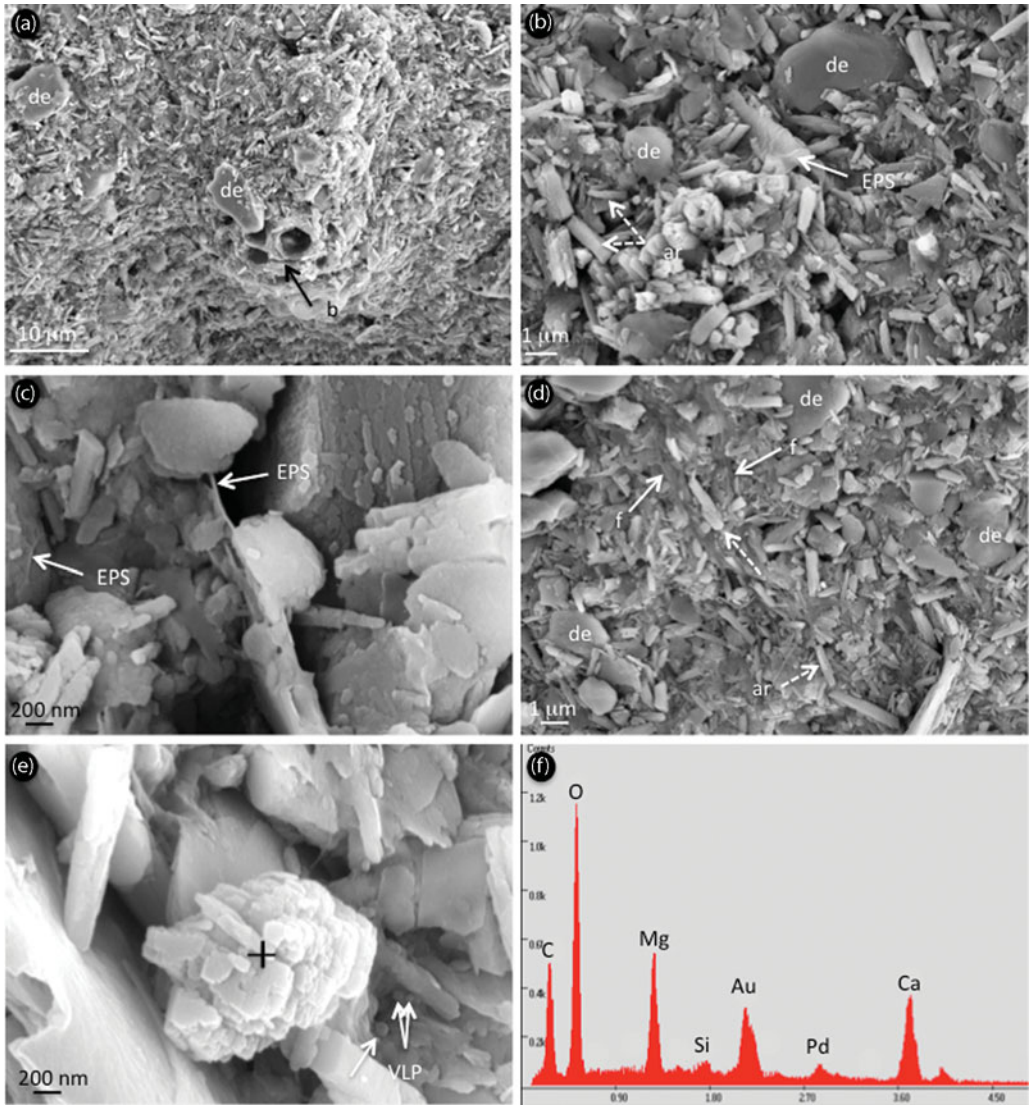

Figure 8. (Colour online) SEM photomicrographs showing microfossils and microstructure of precipitates from Unit III: (a) *B. braunii* ('b') and abundant detrital particles ('de'); (b) detrital particles ('de'), aragonite rods (dashed arrows) and EPS (white arrow); (c) EPS as nanofilaments (arrows); (d) filamentous microbes ('f'), abundant detrital particles ('de') and aragonite ('ar'); (e) nanometre-sized virus-like particles (VLP, arrows) and rhomboedra of Mg-carbonates; and (f) elemental analysis of the Mg-carbonate rhomboedra showing small amount of Si.

microbes and the degradation of figured elements by microbial activity. However, EPS exhibit a different aspect in sediments from Unit IV. They are abundant and characterized by a typical alveolar network (with different orders of magnitude), which can only be preserved when associated with a biofilm or a microbial mat structure (Pacton, Fiet & Gorin, 2007). In that case they are believed to enhance OM preservation, and to provide an efficient chemical and physical barrier against degradation (Pacton, Fiet & Gorin, 2007). This is confirmed by the higher abundance of EPS in Unit IV compared to other units (e.g. Fig. 9), along with the unusual preservation of numerous colonies of coccoid prokaryotes (Fig. 9) and the preserved intracellular content of some cyanobacteria (Fig. 6). EPS are disconnected in sediments from Unit V, while they are more closely associated with Mg-carbonate crystals in the lowermost interval of Unit V.

Microscopical investigations conducted in the different units would suggest a wide abundance of SRB over depth, while archaea distribution may suggest specific ecological niches. Indeed, the cell aggregates observed in the organic layers of Unit III are similar to syntrophic (i.e. metabolic cross-feeding) colonies of bacteria intertwined with filamentous archaea (Stams & Plugge, 2009), which points to anaerobic oxidation of methane (AOM). AOM metabolic process is assumed to be a reversal of methanogenesis, coupled with the reduction of sulphate to sulphide involving methanotrophic archaea (ANME) and sulphate-reducing bacteria (SRB) as syntrophic partners (e.g. Hansen *et al.* 1998; Boetius *et al.* 2000; Valentine & Reeburgh, 2000; Schubert *et al.* 2011). Recent studies have established that at least two phylogenetically different groups of anaerobic methanotrophic Archaea (ANME-I and ANME-II) can mediate this process but seem more sensitive to

https://doi.org/10.1017/S0016756814000831 Published online by Cambridge University Press

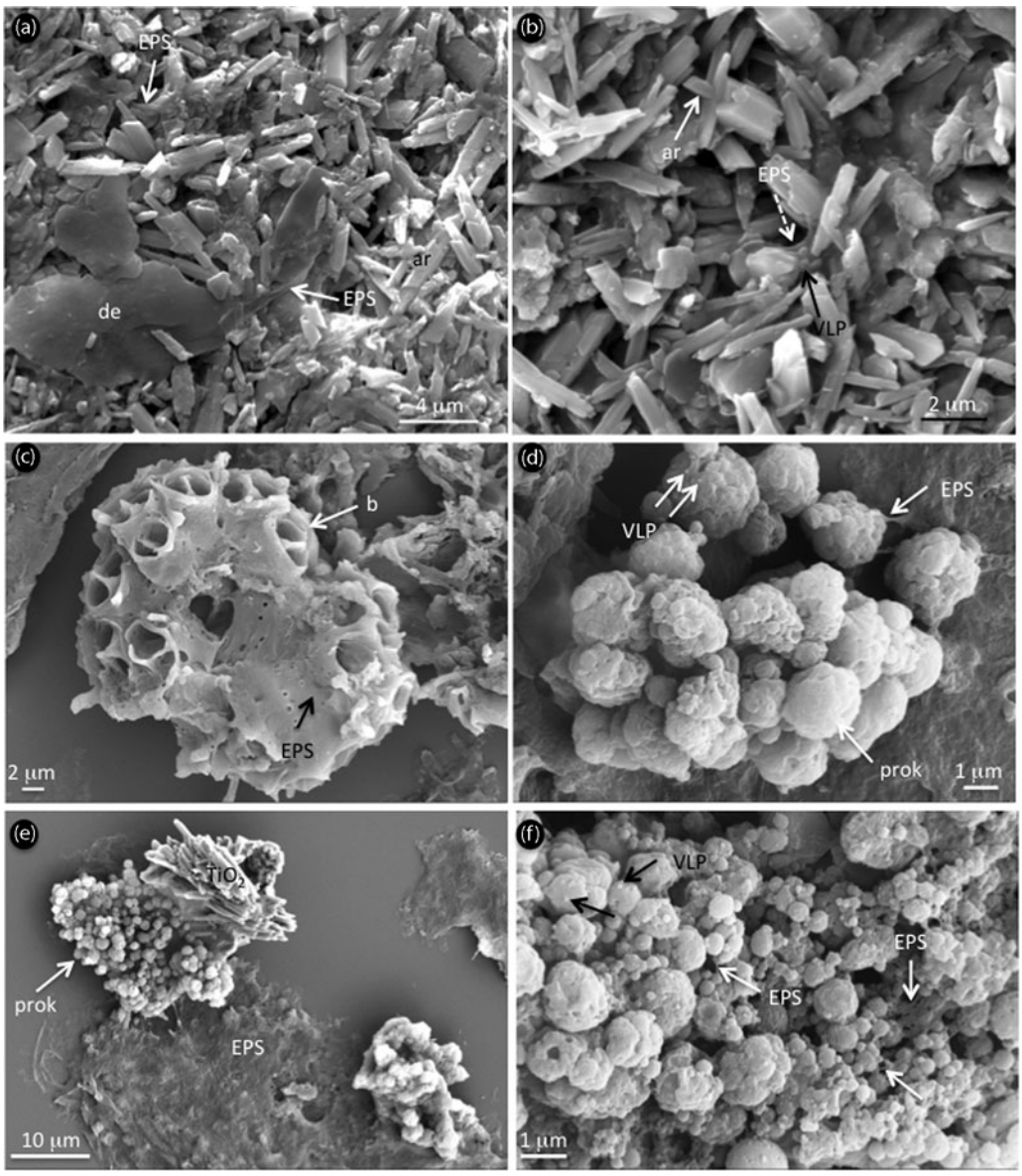

Figure 9. SEM photomicrographs showing (a, b) microfossils and microstructure of precipitates and (c) organic matter after acid etching in the dark greyish layer and in the light-coloured layer from Unit IV. (a) EPS (arrows) covering aragonite crystals ('ar') and detrital particles ('de'); (b) needle-like aragonite crystals ('ar'), nanometre-sized virus-like particles (VLP, black arrow) trapped within EPS (dashed arrow); (c) partially degraded *B. braunii* ('b') covered by EPS (dark arrow); (d) enlargement of coccoid prokaryotes ('prok', see square in supplementary Fig. S3d) closely associated with EPS and nanometre-sized virus-like particles (VLP); (e, f) abundant coccoid prokaryotes closely associated with degraded cuticles and alveolar EPS. Note the presence of rutile in (e) and VLP attached to prokaryotic cells in (f).

temperature rather than to sulphate concentration, pH and salinity, especially in cold conditions for ANME-II (Nauhaus *et al.* 2005). This consortium is likely highly active in Unit IV. The typical EPS distribution, in addition to the well-preserved microbial bodies, would indicate that these communities were living in biofilms or in microbial mat-like structures (e.g. Pacton, Fiet & Gorin, 2006). The higher microbial activity recorded in Unit IV might be explained by microbial community structures and potentially anaerobic methanotrophs-associated phylogeny (Vigneron *et al.* 2013). The presence of intact cyanobacterial cells showing intracellular thylakoid membranes implies that they were fossilized *in situ*, as photosynthetic organisms are rapidly degraded after death in the water column by chemical and physical processes. Such exceptional preservation conditions occur in places where degradation reactions are reduced, as is the case in EPS in microbial mats or biofilms (Pacton, Fiet & Gorin, 2007, 2008). The presence of different aerobic and anaerobic prokaryotic metabolims (i.e. cyanobacteria, SRB and archaea) points to a vertical microbial distribution profile, such as in microbial mats. This microbial community structure can be compared with microbial mat systems such as those reported from Arctic saline coldwater springs (Vincent *et al.* 2009). In such

https://doi.org/10.1017/S0016756814000831 Published online by Cambridge University Press

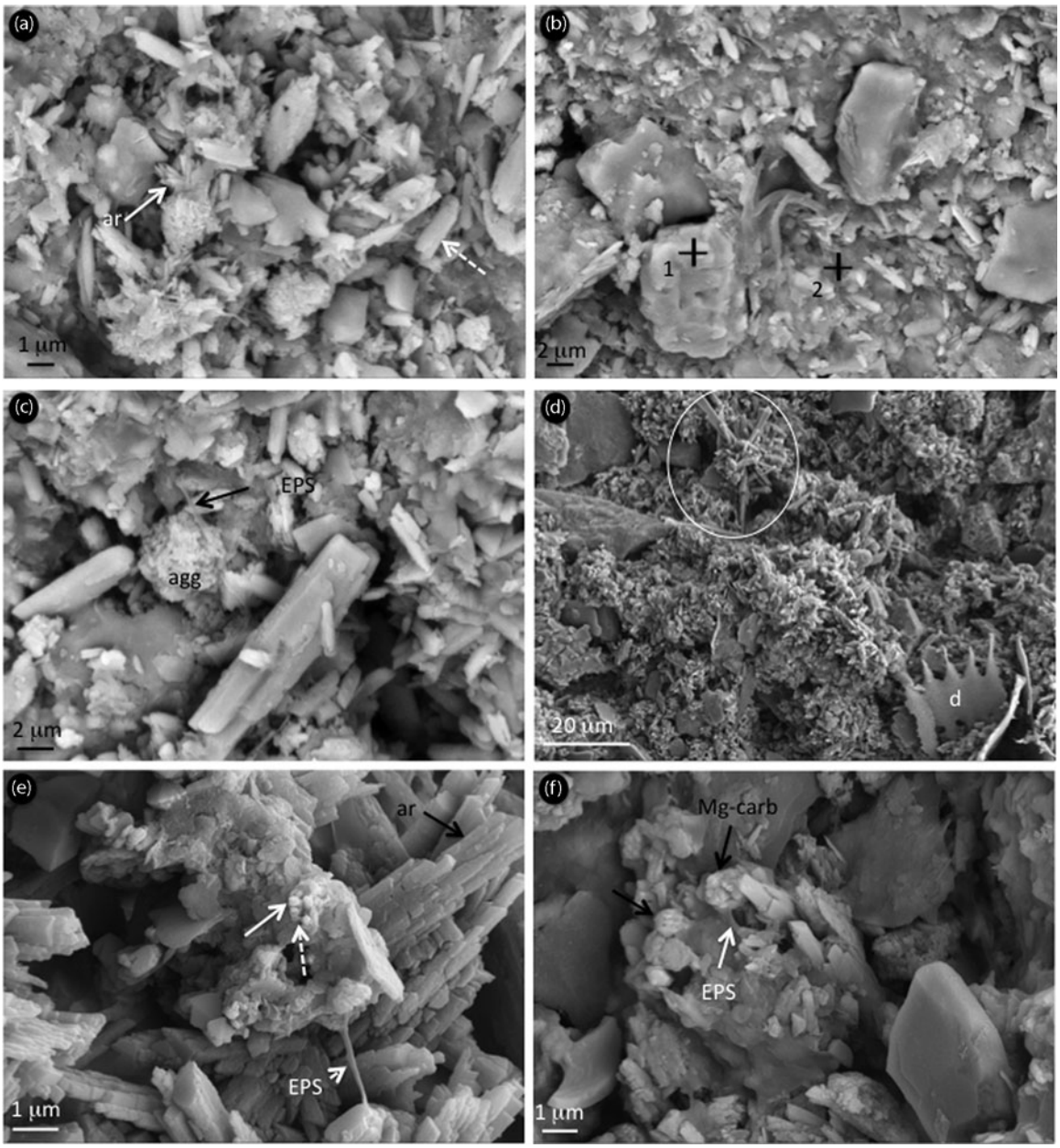

Figure 10. SEM photomicrographs showing microfossils and microstructure of precipitates from Unit V. (a) Spherulite-like aragonite ('ar', arrow) and aragonite rods (dashed arrow); (b) microbial carbonate (1) and mineralized EPS (2); (c) filaments of EPS (black arrows) and associated Mg-carbonate aggregate; (d) aragonite star (circle) and remains of diatoms ('d'); (e) fibrous aragonite ('ar', dark arrow) and tiny carbonate rhombs (white arrow) associated with EPS (dashed arrow) showing sometimes filamentous structures (small arrow); and (f) tiny crystals of microbial Mg-carbonates (dark arrows) embedded within EPS (white arrow).

microbial mats, evidence of AOM was found below the photosynthetic layer of the mat community due to the coexistence of methanogens and SRB (Buckley, Baumgartner & Visscher, 2008).

The composition and structure of microbial communities in Son Kul sediments is quite variable, as demonstrated by the restricted occurrence of microbial mats in Unit IV. In other units, microbes were presumably distributed either in the water column or at the water–sediment interface. In some specific conditions, bacteria can establish connections to terminal electron acceptors through so-called 'nanowires', extensions of the outer membrane and periplasm (Pirbadian *et al.* 2014). Initially described as connectors to other cells in anoxic conditions, nanowires facilitate the transport of electron acceptors between bacteria (Reguera *et al.* 2005). Electrically conductive nanowires are not restricted to metal-reducing bacteria, such as *Shewanella* sp. and *Geobacter* sp., but are also produced by an oxygenic photosynthetic cyanobacterium and a thermophilic fermentative bacterium (Gorby *et al.* 2006). Recent studies suggested that interspecies electron transfer in AOM coupled to bacterial sulphate reduction might be mediated by direct cell–cell contact through nanowires (Thauer & Shima, 2008; Meulepas *et al.* 2010). Further studies are required to assess the

https://doi.org/10.1017/S0016756814000831 Published online by Cambridge University Press

precise role of nanowires in these sediments, for example if they constitute a microbial strategy to the limitation of sulphates.

5.a.2. Virus-like particles

Numerous virus-like particles were found in sediments from Lake Son Kul not only in upper sediments but also in deeper layers (e.g. 88–90 cm; *c.* 5000 BP). Although viruses are ubiquitous components of aquatic systems (e.g. Suttle, 2007; Yau *et al.* 2011), little is known about their preservation potential in the geological record. The lack of viruses in the geological record is attributed to their small size and lack of a unique chemical or isotopic signature (Kyle, Pedersen & Ferris, 2008). Previous studies have shown that viral abundance is strong in oxygenated layers from the upper 40 cm of freshwater sediments (Fischer *et al.* 2003). Viruses were also found in larger abundances in top sediments than in the water column of a temperate lake (Duhamel & Jacquet, 2006), but no data have been yet reported from deeper layers. Viral abundance and distribution was indeed reported from deep-marine sub-seafloor settings, in which genetic material was still present in the capsid (Bird *et al.* 2001; Middelboe, Glud & Filippini, 2011). Fossilized viruses are scarcely reported in the literature, and are found either (1) in acidic waters of the Rio Tinto in Spain (Kyle, Pedersen & Ferris, 2008); (2) being silicified either in laboratory experiments (e.g. Orange *et al.* 2011) or in geothermal systems (Peng *et al.* 2013); or (3) being mineralized as Mg-carbonates in photosynthetic microbial mats (Pacton *et al.* 2014). The identification of fossilized viruses in the geological record therefore remains a challenge. Several lines of evidence must support their origin, including size and morphology, while ruling out potential inorganic precipitates. VLPs described in Lake Son Kul sediments match the criteria for identifying fossilized viruses (Pacton *et al.* 2014), that is, organic nanospheres of size range 20–200 nm, bearing a hexagonal outline that resembles a polyhedral (termed icosahedral) capsid sometimes with a tail attached to it, thus strongly supporting a viral origin. VLPs in surface sediments (e.g. Unit I) are characterized by a capsid full of organic content which is likely genetic material, whereas those from Unit IV look empty suggesting that they probably lost their nucleic acids and that only capsids can be preserved in sediments under anoxic conditions. Viruses are considered to play a key role in the food web as they liberate OM from host cells releasing essential nutrients into the ecosystem (Fuhrman, 1999; Wilhelm & Suttle, 1999; Middelboe & Jørgensen, 2006). This is in agreement with a higher primary productivity in Units I and IV, as shown by high total organic content (TOC) and elevated content in amorphous OM (Huang *et al.* 2014; Mathis *et al.* 2014). High content in amorphous OM is commonly used as a proxy for low oxygen content at the sediment–water interface. It also provides evidence for high primary productivity in the photic zone (Prasad *et al.* 2007; Pacton, Gorin & Vasconcelos, 2011). High viral abundance but low virus-to-bacterium ratios were also reported in freshwater lake sediments (e.g. Maranger & Bird, 1996; Lemke *et al.* 1997). Although sediments favour the preservation of viruses but not their proliferation in tropical environments (Bettarel *et al.* 2006), our data would point to a similar process in cold, high-altitude environments.

5.b. Mineral biosignatures

5.b.1. Carbonates

In lacustrine systems authigenic carbonate phases reveal key environmental information (e.g. sub-annual precipitation signals, lake productivity, low lake level stages, etc.); however, their primary and possible diagenetic origin may blur the interpretation (Talbot & Kelts, 1986). Calcium carbonates in Lake Son Kul sediments are mainly dominated by aragonite (except for Unit II), with lower contributions of Mg-calcite and dolomite.

5.b.1.a. Aragonite

Whether the origin of aragonite in sediments is inorganic or biological is still under debate (DeGroot, 1965; Shinn *et al.* 1989; Boss & Neumann, 1993; Milliman *et al.* 1993; Morse, Gledhill & Millero, 2003), but most of these studies are related to warm- and shallow-marine environments. Aragonite formed in cold, oligotrophic, high-latitude settings (e.g. Antarctica; see Hendy *et al.* 1979; Lawrence & Hendy, 1985; Bird *et al.* 1991; Hendy, 2000) or in montane lakes is highly unusual, and has only been reported in Bear Lake (USA) associated with an increase in salinity (Dean *et al.* 2006). The key variable for aragonite formation appears to be a high Mg:Ca ratio (Müller, Irion & Förstner, 1972), and an increase in Mg:Ca ratio is usually accompanied by an increase in salinity (Kelts & Hsü, 1978). In lake environments, the occurrence of algal blooms in the epilimnion promotes carbonate precipitation by reducing CO_2 concentrations, which leads to increasing pH values (e.g. Kelts & Hsü, 1978; Koschel *et al.* 1983; Koschel, 1997). This mechanism is therefore considered as a biologically induced precipitation pathway. Micrometre-sized needle-like particles in Son Kul sediments are similar to those reported from algal blooms (e.g. Hodell *et al.*, 1998; Sondi & Juracic, 2010), suggesting a similar process linked to biological productivity in the lake.

However, whether primary productivity was primarily driven by photosynthetic organisms or by chemotrophic prokaryotes (such as methanogens) remains unknown. The highest content in aragonite is recorded in Unit IV, and corresponds to the clear occurrence of SRB and methanotrophic archaea as consortia. Stable carbon isotopes values on bulk carbonates from Units IV and V are slightly depleted ($\delta^{13}C$ of −2 to 4 ‰ compared to the upper units of $\delta^{13}C$ of 4–8 ‰; Huang *et al.* 2014), suggesting that AOM (inducing light $\delta^{13}C$) contributed to carbon mineralization prior to (Mg-)calcite

https://doi.org/10.1017/S0016756814000831 Published online by Cambridge University Press

precipitation; this is in contrary to methanogenesis producing CO_2 enriched in ^{13}C (Waldron, Hall & Fallick, 1999; Jahren, LePage & Werts, 2004; Chanton *et al.* 2005). Such $\delta^{13}C_{carb}$ values in Unit IV and V are similar to those from Lake Cadagno where AOM is an important process in the carbon cycle (Schubert *et al.* 2011). Additionally, a new morphotype of aragonite appears in Units IV and V, consisting of micrometre-sized elongated rod- to radial-star-shaped crystal aggregates. This morphotype is similar to the star-shaped type 1 spherulite illustrated in Andreassen, Beck & Nergaard (2012), which evolves to spherulites by increasing the supersaturation. The star-shaped morphotype further resembles spherulite precursors similar to those found in microbial mats and stromatolites (e.g. Spadafora *et al.* 2010). Aragonite spherulites have also been reported associated with bacteria as a tracer of increased salinity (Sanchez-Navas *et al.* 2009) and are frequently found in (hyper)saline environments (Spadafora *et al.* 2010; Arp *et al.* 2012). Whether these precipitates are of organic or inorganic origin remain unknown. However, as EPS are of relative importance in Unit IV (a major constituent of microbial mats) and in Unit V, they might have influenced the formation of star-shaped minerals in both units. At Lake Issyk-Kul (Kyrgyzstan) a similar microbial process was proposed for the possible origin of vaterite, a polymorph of $CaCO_3$ (Giralt, Julia & Klerkx, 2001).

5.b.1.b. Dolomite

Dolomite in sediments is one of the most controversial topics in sedimentary geology (e.g. Warren, 2000; McKenzie & Vasconcelos, 2009). This is mostly because no precipitation of dolomite has been rigorously demonstrated in laboratory experiments at low temperatures and in the absence of microbial activity (Lippmann, 1973; Land, 1998). More specifically, the metabolic activity of SRB has so far been considered to overcome the kinetic barrier to dolomite formation by increasing pH and carbonate alkalinity (Vasconcelos *et al.* 1995; Warthmann *et al.* 2000), although recent studies showed that sulphate reduction is not sufficient to induce carbonate precipitation in microbial mats (Meister, 2013). Microbial dolomite is widely encountered in modern saline environments (e.g. Vasconcelos & McKenzie, 1997; Wright, 1999; Wright & Oren, 2005; Wright & Wacey, 2005), while biogenic dolomite precipitation was observed in non-hypersaline inland lakes (Deng *et al.* 2010) and in freshwater experiments, more specifically associated with methanogenic waters (Roberts *et al.* 2004; Kenward *et al.* 2009). Dolomite precipitation can occur around cells (Warthmann *et al.* 2000) or associated with EPS (Sanchez-Roman *et al.* 2008; Deng *et al.* 2010) produced by SRB. Recently, the precipitation of dolomite was shown closely associated with cyanobacterial EPS and organic carbon, while SRB influence was not excluded (Paulo & Dittrich, 2013). However, a variety of microbes other than SRB can trigger dolomite precipitation such as methanogens (Roberts *et al.* 2004; Kenward *et al.* 2009), sulphide-oxidizing bacteria (Moreira *et al.* 2004) and methane-oxidizing archaea in gas hydrate deposits (Sassen *et al.* 2004). Dolomite in Son Kul sediments is more abundant in the light-coloured layers from Units I, II (up to 9 %) and V, while this pattern is more complex in the finely laminated sediments of Unit IV. In the latter, FISH data combined with dolomite occurrences (based on XRD analyses) indicate that the highest dolomite content was recorded close to clear occurrences of SRB/archaea consortia in sediments. However, the wide presence of EPS in these samples precludes the discrimination of methanotrophic archaea coupled with SRB from passive mineralization of EPS (cf. Bontognali *et al.* 2014) as the main process triggering dolomite precipitation. We propose that dolomite most probably formed in the early diagenetic phase, similar to the other Mg-calcite crystals, when pore water was highly mineralized. It must also be considered that dolomite might be a byproduct related to methanogenesis occurring in soils around the lake (as it has been reported from other lake systems; e.g. Talbot & Kelts, 1986), although we cannot rule out the possibility that methanogenesis operated in the lake itself. Monitoring surveys in the 1960s and 1970s indeed reported nearshore emanations of H_2 and methane during the cold season (Beloglasova & Smirnova, 1987). Considering that core SK07 is a proximal site in Lake Son Kul (therefore with a proximal habitus), the influence of both surface and groundwater inputs of soil-derived methanogenesis-related products on the formation of authigenic carbonates in lake sediments should be considered.

5.b.2. Iron sulphides

Framboidal pyrites have been widely encountered in Son Kul sediments but in Units I and II only, and are almost absent from the underlying units. Numerous studies have demonstrated that the growth of framboidal pyrite at temperatures above 60 °C can occur in abiotic laboratory systems (e.g. Ohfuji & Rickard, 2005). They are widely found in natural sedimentary environments, although the formation processes are still unclear (Ohfuji & Rickard, 2005), supporting a biological origin (e.g. Sawlowicz, 2000; Popa, Badescu & Kinkle, 2004; Vuillemin *et al.* 2013). More specifically, the presence of framboidal pyrites reflect precipitation from highly supersaturated fluids developed due to metabolic activity of sulphate-reducing bacteria (Habicht & Canfield, 1997; Wilkin & Barnes, 1997; Maclean *et al.* 2008). Pyrite sulphur is provided by microbial sulphate reduction (Berner, 1984) increasing the alkalinity of the pore water according to the reaction

$$2CHO + SO_4^{2-} \rightarrow H_2S + 2HCO_3^{2-} \quad (1)$$

H_2S produced by sulphate reduction may react with Fe^{2+} leading to precipitation of aggregates of pyrite:

$$2H_2S + Fe^{2+} \rightarrow FeS_2 + 2H^+ \quad (2)$$

https://doi.org/10.1017/S0016756814000831 Published online by Cambridge University Press

Precipitation of pyrite was also shown to be a common byproduct of sulphate reduction and AOM (Schink, 2002). However, FISH surveys in Son Kul sediments showed that AOM occurred mainly in both Units IV and V, suggesting that framboidal pyrites may have been mediated through sulphate reduction only. The lack of framboidal pyrite in Unit IV may be linked to either oxidation of initially formed pyrite, inhibition of crystallization caused by sulphate limitation or a lack of reactive iron availability. Considering the first hypothesis, oxidation of pyrite would have generated an acidic sulphur-rich solution (e.g. Blowes & Jambor, 1990; Edwards *et al.* 2000) that would have been buffered by carbonates. In such case, we would expect to find sulphates and iron oxi-hydroxides (e.g. Charpentier *et al.* 2004) or even smectite (Gaudin *et al.* 2005). However, none of these minerals was found to be significantly higher in Units IV and V compared to Units I and II. Inhibition of pyrite crystallization is therefore the most likely hypothesis. Unit IV is characterized by the highest abundance of syntrophic consortia of sulphate-reducing bacteria and methanotrophic archaea (Fig. 6; Section 5.a.1). They catalyse the reaction:

$$CH_4 + SO_4^{2-} \rightarrow HCO_3^- + HS^- + H_2O \qquad (3)$$

(Hinrichs *et al.* 1999; Boetius *et al.* 2000; Orphan *et al.* 2001; Knittel *et al.* 2005; Niemann *et al.* 2006) and do not favour a sulphate limitation as the main factor preventing pyrite formation. Consequently, the absence of reactive iron availability seems to be the most likely explanation for the absence of framboidal pyrite in Units III, IV and V in core SK07.

5.b.3. Stomatocysts

Biogenic siliceous microspheres, referred to as chrysophyte stomatocysts, have been found in the different units from core SK07. Although they display various morphologies, stomatocyst 52 (produced by more than one species; Duff, Zeeb & Smol, 1995) seems to dominate microfossil assemblages. These stomatocysts were found elsewhere in arctic and alpine habitats such as arctic tundra lakes, arctic peats, arctic ponds, alpine ponds and montane lakes, suggesting that stomatocysts are produced by a cold-tolerant form. Chrysophyte stomatocysts (Smol, 1988), and silica-scaled chrysophytes (Wilken, Kristiansen & Jürgensen, 1995) accumulate in sediments and are used to reconstruct past climate trends, especially in cold regions (Charvet, Vincent & Lovejoy, 2012). Previous studies have shown that chrysophytes respond to a variety of environmental changes, including shifts in pH (Duff & Smol 1991; Facher & Schmidt 1996; Wilkinson, Hall & Smol, 1999), trophic status (Zeeb, Duff & Smol, 1990; Zeeb *et al.* 1994; Wilkinson, Hall & Smol, 1999; Cabala & Piatek, 2004; Charvet, Vincent & Lovejoy, 2012), salinity (Pienitz *et al.* 1992; Zeeb & Smol, 1995), pronounced seasonal changes in light availability (Charvet, Vincent & Lovejoy, 2012) and climate (Zeeb & Smol, 1993). Their success is most likely due to their diverse nutritional strategies and ability to produce resistant siliceous resting stages, termed stomatocysts. Unlike most other algal groups that are predominantly autotrophic, many chrysophytes are able to switch between autotrophy, heterotrophy and even phagotrophy. Moreover, their ability to create a resilient resting stage allows them to survive unfavourable conditions (Betts-Piper, Zeeb & Smol, 2004). According to Holmgren (1984), Lake Son Kul falls into the Chrysophyceae-diatoms assemblage classification. Although unornamented cysts are widely distributed across a variety of geographical and ecological gradients (Betts-Piper, Zeeb & Smol, 2004), the abundance of these morphotypes in Holocene sediments at Son Kul suggests that ecological conditions were continuously favourable for their growth (at least in Units I and II) in this cold, alpine lake during Holocene time. Further investigations are nevertheless required to study the variations in stomatocyst assemblages over depth, in order to more precisely evaluate palaeoenvironmental conditions in Lake Son Kul during the Holocene.

6. Summary and conclusions

This work demonstrates the high potential of coupling a geomicrobiological approach to a classical facies analysis for the study of laminated lacustrine sediments. Microbe–mineral interactions investigated in sediments from Lake Son Kul reveal different environmental processes in which microbes played a fundamental role (Table 1). Microbial communities are dominated by SRB at the water–sediment interface, degrading OM. They promoted dolomite and framboidal pyrite precipitation during early diagenesis. Moreover, SRB lived in consortia with methanotrophic archaea and performed AOM, especially between 7000 and 5000 BP when microbial mat structures producing large quantities of EPS enhanced the preservation of microbial structures such as virus-like particles and coccoid prokaryotes. Aragonite is of primary origin and driven by biological activity similar to algal bloom events (especially in Unit IV). Moreover, another morphotype of aragonite (a spherulite-like precursor) occurs in Unit IV, possibly mediated by EPS in microbial mats. This study further highlights that the preservation of Holocene viral relics at Lake Son Kul can provide promising and new perspectives in the search for viral biosignatures in ancient sediments.

Acknowledgements. The authors thank two anonymous reviewers for their constructive comments. The authors acknowledge Daniel Ariztegui for conducting micro-XRF elemental mappings (University of Geneva) and the Centre Technologique des Microstructures (University Claude Bernard-Lyon 1) for electron microscopy facilities. We thank Lydia Zehnder (ETH Zurich) for her support with X-ray diffraction analysis. We are also grateful to Samuel Mailliot (University Lyon1) for his contribution to Figure 1 and Tharsis-Energy for financial support.

Table 1. The main biogeochemical processes taking place in Core SK07 from Lake Son Kul (with associated specific minerals and biominerals) for lithological Units I–V.

Unit	Facies characteristics	Minerals	Biominerals	Microbial influence	Main biogeochemical processes
I	Light laminae and greyish laminae	Aragonite (slightly enriched in light-coloured laminae), Mg-calcite, dolomite and gypsum	Framboidal pyrite; Mg-carbonate associated with EPS	Microbes degrading terrestrial OM; more abundant SRB in greyish laminae with local AOM consortia compared to some SRB clusters in light laminae	Aragonite driven by algal bloom; framboidal pyrite mediated by SRB; dolomite induced by SRB
II	Dark carbonaceous mud	Mainly detrital minerals with gypsum, dolomite, calcite and aragonite	Framboidal pyrite	Microbes degrading terrestrial OM; rare SRB and archaea	Framboidal pyrite mediated by SRB; dolomite induced by SRB
III	Clays and organic-rich mud	Mainly aragonite and detrital minerals, gypsum and few dolomite and Mg-calcite	Mg-carbonate	Microbes degrading terrestrial OM; rare SRB and archaea	Aragonite driven by algal blooms; dolomite induced by SRB
IV	Alternation of micritic aragonite laminae and organic Fe-rich laminae	*c.* 70 % of aragonite, absence of dolomite in white laminae, low Mg-calcite, gypsum and detrital minerals	Star-shaped aragonite; Mg-carbonate associated with EPS	Microbes degrading terrestrial and algal OM; microbial mats; AOM in dark laminae (coccoid prokaryotes); SRB dominating over archaea in aragonite laminae (with local consortia)	Star-shaped aragonite mediated by EPS and/or supersaturation; dolomite induced or influenced by SRB and their EPS
V	Grey carbonaceous mud	Mainly aragonite and detrital minerals, gypsum and few dolomite and Mg-calcite	Star-shaped aragonite; Mg-carbonate associated with EPS	Microbes degrading terrestrial OM; abundance of SRB clusters; rare archaea	Star-shaped aragonite mediated by EPS and/or supersaturation; dolomite induced or influenced by SRB and their EPS

Supplementary material

To view supplementary material for this article, please visit http://dx.doi.org/10.1017/S0016756814000831

References

AMANN, R. I., LUDWIG, W. & SCHLEIFER, K-H. 1995. Phylogenetic identification and in situ detection of individual microbial cells without cultivation. *Microbiological Reviews* **59**, 143–69.

AMANN, R. I., KRUMHOLZ, L. & STAHL, D. A. 1990. Fluorescent-oligonucleotide probing of whole cells for determinative, phylogenetic, and environmental studies in microbiology. *Journal of Bacteriology* **172**, 762–70.

ANDREASSEN, J.-P., BECK, R. & NERGAARD, M. 2012. Biomimetic type morphologies of calcium carbonate grown in absence of additives. *Faraday Discussion* **159**, 247–61.

ARP, G., HELMS, G., KARLINSKA, K., SCHUMANN, G., REIMER, A., REITNER, J. & TRICHET, J. 2012. Photosynthesis versus exopolymer degradation in the formation of microbialites on the atoll of Kiritimati, Republic of Kiribati, Central Pacific. *Geomicrobiology Journal* **29**, 29–65.

BANFIELD, J. F., MOREAU, J. W., CHAN, C. S., WELCH, S. A. & LITTLE, B. 2001. Mineralogical biosignatures and the search for life on Mars. *Astrobiology* **1**, 447–63.

BELOGLASOVA, V. N. & SMIRNOVA, N. B. 1987. *Altas Kirgizskoj SSR*. GUGK SSSR, Bishkek (in Russian).

BERNER, R. A. 1984. Sedimentary pyrite formation: An update. *Geochimica et Cosmochimica Acta* **48**, 605–15.

BETTAREL, Y., BOUVY, M., DUMONT, C. & SIME-NGANDO, T. 2006. Virus-bacterium interactions in water and sediment of West African inland aquatic systems. *Applied and Environmental Microbiology* **72**, 5274–82.

BETTS-PIPER, A. M., ZEEB, B. A. & SMOL, J. P. 2004. Distribution and autoecology of chrysophyte cysts from high Arctic Svalbard lakes: preliminary evidence of recent environmental change. *Journal of Paleolimnology* **31**, 467–81.

BIRD, D. F., JUNIPER, S. K., RICCIARDI-RIGAULT, M., MARTINEU, P., PRAIRIE, Y. T. & CALVERT, S. E. 2001. Subsurface viruses and bacteria in Holocene/Late Pleistocene sediments of Saanich Inlet, BC: ODP holes 1033B and 1043B, Leg 169S. *Marine Geology* **174**, 227–39.

BIRD, M. I., CHIVAS, A. R., RADNELL, C. J. & BURTON, H. R. 1991. Sedimentological and stable-isotope evolution of lakes in the Vestfold Hills, Antarctica. *Palaeogeography, Palaeoclimatology, Palaeoecology* **84**, 109–30.

BLOWES, D. W. & JAMBOR, J. L. 1990. The pore-water geochemistry and the mineralogy of the vadose zone of sulfide tailings, Waite Amulet, Quebec, Canada. *Applied Geochemistry* **5**, 327–46.

BOETIUS, A., RAVENSCHLAG, K., SCHUBERT, C., RICKERT, D., WIDDEL, F., GIESEKE, A., AMANN, R., JØRGENSEN, B. B., WITTE, U. & PFANNKUCHE, O. 2000. A marine microbial consortium apparently mediating anaerobic oxidation of methane. *Nature* **407**, 623–6.

BONTOGNALI, T. R. R., MCKENZIE, J. A., WARTHMANN, R. J. & VASCONCELOS, C. 2014. Microbially influenced formation of Mg-calcite and Ca-dolomite in the presence of exopolymeric substances produced by sulphate-reducing bacteria. *Terra Nova* **26**, 72–7.

BOSS, S. K. & NEUMANN, A. C. 1993. Physical versus chemical processes of whiting formation in the Bahamas. *Carbonates Evaporites* **8**, 135–48.

BRAUER, A., ALLEN, J. R. M., MINGRAM, J., DULSKI, P., WULF, S. & HUNTLEY, B. 2007. Evidence for last interglacial chronology and environmental change from southern Europe. *PNAS* **104**(2), 450–55.

BUCKLEY, D. H., BAUMGARTNER, L. K. & VISSCHER, P. T. 2008. Vertical distribution of methane metabolism in microbial mats of the Great Sippewissett Salt Marsh. *Environmental Microbiology* **10**, 967–77.

CABALA, J. & PIATEK, M. 2004. Chrysophycean stomatocysts from the Staw Toporowy Nizni lake (Tatra National Park, Poland). *Annales de Limnologie – International Journal of Limnology* **40**, 149–65.

CHANTON, J. L., CHASER, P., GLASSER, D. & SIEGEL, 2005. Carbon and hydrogen isotopic effects in microbial methane from terrestrial environments. Chapter 6. In *Stable Isotopes and Biosphere - Atmosphere Interactions: Processes and Biological Controls* (eds L. B. Flanagan, J. R. Ehleringer & D. E. Pataki), pp. 85–112. Amsterdam: Elsevier.

CHARPENTIER, D., MOSSER-RUCK, R., CATHELINEAU, M. & GUILLAUME, D. 2004. Oxidation of mudstone in a tunnel (Tournemire, France): consequences on mineralogy and crystal chemistry of clay minerals. *Clay Mineralogy* **39**, 135–49.

CHARVET, S., VINCENT, W. F. & LOVEJOY, C. 2012. Chrysophytes and other protists in High Arctic lakes: molecular gene surveys, pigment signatures and microscopy. *Polar Biology* **35**, 733–48.

DEAN, W., ROSENBAUN, J., SKIPP, G., COLMAN, S., FORESTER, R., LIU, A., SIMMONS, K. & BISCHOFF, J. 2006. Unusual Holocene and late Pleistocene carbonate sedimentation in Bear Lake, Utah and Idaho, USA. *Sedimentary Geology* **185**, 93–112.

DEGROOT, K. 1965. Inorganic precipitation of calcium carbonate production from seawater. *Nature* **207**, 404–5.

DENG, S., DONG, H., LV, G., JIANG, H., YU, B. & BISHOP, M. E. 2010. Microbial dolomite precipitation using sulfate reducing and halophilic bacteria: Results from Qinghai Lake, Tibetan Plateau, NW China. *Chemical Geology* **278**, 151–9.

DUFF, K. E. & SMOL, J. P. 1991. Morphological descriptions and stratigraphic distributions of the chrysophycean stomatocysts from a recently acidified lake (Adirondack Park, N.Y.). *Journal of Paleolimnology* **5**, 73–113.

DUFF, K. E., ZEEB, B. A. & SMOL, J. P. 1995. *Atlas of Chrysophycean Cysts*. Dordrecht: Kluwer Academic Publishers, 189 pp.

DUHAMEL, S. & JACQUET, S. 2006. Flow cytometric analysis of bacteria- and virus-like particles in lake sediments. *Journal of Microbiological Methods* **64**, 316–22.

DUPRAZ, C., REID, R. P., BRAISSANT, O., DECHO, A. W., NORMAN, R. S. & VISSCHER, P. T. 2009. Processes of carbonate precipitation in modern microbial mats. *Earth Science Reviews* **6**, 141–62.

EDWARDS, K. J., BOND, P. L., DRUSCHEL, G. K., MCGUIRE, M. M., HAMERS, R. J. & BANFIELD, J. F. 2000. Geochemical and biological aspects of sulfide mineral dissolution: lessons from Iron Mountain, California. *Chemical Geology* **169**, 383–97.

FACHER, E. & SCHMIDT, R. 1996. A siliceous chrysophycean cyst-based pH transfer function for Central European Lakes. *Journal of Paleolimnology* **16**, 275–321.

FISCHER, U. R., WIELTSCHNIG, C., KIRSCHNER, A. K. T. & VELIMIROV, B. 2003. Does virus-induced lysis contribute significantly to bacterial mortality in the oxygenated sediment layer of shallow oxbow lakes? *Applied and Environmental Microbiology* **69**, 5281–9.

FLÜGEL, E. 2004. *Microfacies of Carbonate Rocks. Analysis, Interpretation and Application*. Berlin, Heidelberg, New York: Springer, 976 pp.

FRANCUS, P., SUCHODOLETZ, H., DIETZE, M., DONNER, R. V., BOUCHARD, F., ROY, A-J., FAGOT, M., VERSCHUREN, D. & KRÖPELIN, S. 2013. Varved sediments of Lake Yoa (Ounianga Kebir, Chad) reveal progressive drying of the Sahara during the last 6100 years. *Sedimentology* **60**, 911–34.

FUHRMAN, J. A. 1999. Marine viruses and their biogeochemical and ecological effects. *Nature* **399**, 541–8.

GAUDIN, A., BUATIER, M. D., BEAUFORT, D., PETIT, S., GRAUBY, O. & DECAREAU, A. 2005. Characterization and origin of Fe3+-Montmorillonite in deep water calcareous sediments (Pacific ocean, Costa Rica margin). *Clays and Clay Minerals* **53**, 452–65.

GIRALT, S., JULIA, R. & KLERKX, J. 2001. Microbial biscuits of vaterite in Lake Issyk-Kul (Republic of Kyrgyzstan). *Journal of Sedimentary Research* **71**, 430–5.

GORBY, Y. A., YANINA, S., MCLEAN, J. S., ROSSO, K. M., MOYLES, D., DOHNALKOVA, A., BEVERIDGE, T. J., CHANG, I. S., KIM, B. H., KIM, K. S., CULLEY, D. E., REED, S. B., ROMINE, M. F., SAFFARINI, D. A., HILL, E. A., SHI, L., ELIAS, D. A., KENNEDY, D. W., PINCHUK, G., WATANABE, K., ISHII, S., LOGAN, B., NEALSON, K. H. & FREDRICKSON, J. K. 2006. Electrically conductive bacterial nanowires produced by Shewanella oneidensis strain MR-1 and other microorganisms. *Proceedings of the National Academy of Sciences of the USA* **103**, 11358–63.

HABICHT, K. S. & CANFIELD, D. E. 1997. Sulfur isotope fractionation during bacterial sulfate reduction in organic-rich sediments. *Geochimica et Cosmochimica Acta* **61**, 5351–61.

HANSEN, L. B., FINSTER, K., FOSSING, H. & IVERSEN, N. 1998. Anaerobic methane oxidation in sulfate depleted sediments: effects of sulfate and molybdate additions. *Aquatic Microbial Ecology* **14**, 195–204.

HENDY, C. H. 2000. Late Quaternary lakes in the McMurdo Sound region of Antarctica. *Geografiska Annaler* **82A**, 411–32.

HENDY, C. H., HEALY, T. R., RAYNER, E. M., SHAW, J. & WILSON, A. T. 1979. Late Pleistocene glacial chronology of the Taylor Valley, Antarctica, and the global climate. *Quaternary Research* **11**, 172–84.

HINRICHS, K. U., HAYES, J. M., SYLVA, S. P., BREWER, P. G. & DELONG, E. F. 1999. Methane consuming archaebacteria in marine sediments. *Nature* **398**(6730), 802–5.

HODELL, D. A., SCHELSKE, C. L., FAHNENSTIEL, G. L. & ROBBINS, L. L. 1998. Biologically induced calcite and its isotopic composition in Lake Ontario. *Limnology and Oceanography* **43**, 187–99.

HOLMGREN, S. K. 1984. Experimental lake fertilization in the Kuokkel area, Northern Sweden: Phytoplankton biomass and algal composition in natural and fertilized subarctic lakes. *Internationale Revue der gesamten Hydrobiologie* **69**, 781–817.

HUANG, X., OBERHÄNSLI, H., VON SUCHODOLETZ, H., PRASAD, S., SORREL, P., PLESSEN, B., MATHIS, M. & USUBALIEV, R. 2014. Hydrological changes in western

Central Asia (Kyrgyzstan) during the Holocene: Results of a paleolimnological study from Son Kul. *Quaternary Science Reviews* **103**, 134–52.

JAHREN, A. H., LEPAGE, B. A. & WERTS, S. P. 2004. Methanogenesis in Eocene Arctic soils inferred from $\delta^{13}C$ of tree fossil carbonates. *Palaeogeography, Palaeoclimatology Palaeoecology* **214**, 347–58.

KELTS, K. & HSÜ, K. J. 1978. Freshwater carbonate sedimentation. In: *Lakes, Chemistry, Geology, Physics* (ed. A. Lerman), pp. 295–323. New York: Springer-Verlag.

KENWARD, P. A., GOLDSTEIN, R. H., GONZALEZ, L. A. & ROBERTS, J. A. 2009. Precipitation of low-temperature dolomite from an anaerobic microbial consortium: the role of methanogenic Archaea. *Geobiology* **7**(5), 556–65.

KNITTEL, K., LÖSEKANN, T., BOETIUS, A., KORT, R. & AMANN, R. 2005. Diversity and distribution of methanotrophic archaea at cold seeps. *Applied and Environmental Microbiology* **71**, 467–79.

KOSCHEL, R. 1997. Structure and function of pelagic calcite precipitation in lake ecosystems. *Verhandlungen des Internationalen Vereins für Limnologie* **26**, 343–9.

KOSCHEL, R., BENNDORF, J., PROFT, G. & RECKNAGEL, F. 1983. Calcite precipitation as a natural control mechanism of eutrophication. *Archiv für Hydrobiologie* **98**(3), 380–408.

KYLE, J. E., PEDERSEN, K. & FERRIS, F. G. 2008. Virus mineralization at low pH in the Rio Tinto, Spain. *Geomicrobiology Journal* **25**, 338–45.

LAND, L. S. 1998. Failure to precipitate dolomite at 25 °C from dilute solutions despite 1000-fold oversaturation after 32 years. *Aquatic Geochemistry* **4**, 361–8.

LAUTERBACH, S., WITT, R., PLESSEN, B., DULSKI, P., PRASAD, S., MINGRAM, J., GLEIXNER, G., HETTLER-RIEDEL, S., STEBICH, M., SCHNETGER, B., SCHWALB, A. & SCHWARZ, A. 2014. Climatic imprint of the mid-latitude Westerlies in the Central Tien Shan of Kyrgyzstan and teleconnections to North Atlantic climate variability during the last 6000 years. *The Holocene* **24**(8), 970–84.

LAWRENCE, M. J. F. & HENDY, C. H. 1985. Water column and sediment characteristics of Lake Fryxell, Taylor Valley, Antarctica. *New Zealand Journal of Geology and Geophysics* **28**, 543–52.

LEMKE, M., WICKSTROM, C. & LEFF, L. 1997. Preliminary study on the distribution of viruses and bacteria in lotic environments. *Archiv für Hydrobiologie* **141**, 67–74.

LIPPMANN, F. 1973. *Sedimentary Carbonate Minerals*. Berlin: Springer-Verlag.

MACLEAN, L. C., TYLISZCZAK, T., GILBERT, P. U., ZHOU, D., PRAY, T. J., ONSTOTT, T. C. & SOUTHAM, G. 2008. A high-resolution chemical and structural study of framboidal pyrite formed within a low-temperature bacterial biofilm. *Geobiology* **6**, 471–80.

MARANGER, R. & BIRD, D. F. 1996. High concentrations of viruses in the sediments of Lac Gilbert, Québec. *Microbial Ecology* **31**, 141–51.

MATHIS, M., SORREL, P., KLOTZ, S., HUANG, X. & OBERHÄNSLI, H. 2014. Regional vegetation patterns at Lake Son Kul reveal Holocene climatic variability in central Tien Shan (Kyrgyzstan, Central Asia). *Quaternary Science Reviews* **89**, 169–85.

MCKENZIE, J. A. & VASCONCELOS, C. 2009. Dolomite Mountains and the origin of the dolomite rock of which they mainly consist: historical developments and new perspectives. *Sedimentology* **56**, 205–19.

MEISTER, P. 2013. Two opposing effects of sulfate reduction on carbonate precipitation in normal marine, hypersaline, and alkaline environments. *Geology* **41**, 499–502.

MEULEPAS, R. J. W., JAGERSMA, C. G., KHADEM, A. F., STAMS, A. J. M. & LENS, P. N. L. 2010. Effect of methanogenic substrates on anaerobic oxidation of methane and sulfate reduction by an anaerobic methanotrophic enrichment. *Applied Microbiology and Biotechnology* **87**, 1499–506.

MIDDELBOE, M., GLUD, R. N. & FILIPPINI, M. 2011. Viral abundance and activity in the deep sub-seafloor biosphere. *Aquatic Microbial Ecology* **63**, 1–8.

MIDDELBOE, M. & JØRGENSEN, N. O. G. 2006. Viral lysis of bacteria: an important source of dissolved amino acids and cell wall components. *Journal of the Marine Biological Association of the UK* **86**, 605–12.

MILLIMAN, J. D., FREILE, D., STEINEN, R. P. & WILBER, R. J. 1993. Great Bahama Bank aragonitic muds: mostly inorganically precipitated, mostly exported. *Journal of Sedimentary Petrology* **63**, 589–95.

MOREIRA, N. F., WALTER, L. M., VASCONCELOS, C., MCKENZIE, J. A. & MCCALL, P. J. 2004. Role of sulfide oxidation in dolomitization: sediment and pore-water geochemistry of a modern hypersaline lagoon system. *Geology* **32**(8), 701–4.

MORSE, J. W., GLEDHILL, D. K. & MILLERO, F. J. 2003. $CaCO_3$ precipitation kinetics in waters from the great Bahama Bank: implications for the relationship-betweenbankhydrochemistry and whitings. *Geochimica et Cosmochimica Acta* **67**, 2819–26.

MÜLLER, G., IRION, G. & FÖRSTNER, U. 1972. Formation and diagenesis of inorganic Ca-Mg carbonates in the lacustrine environment. *Naturwissenschaften* **59**, 158–64.

NAUHAUS, K., TREUDE, T., BOETIUS, A. & KRÜGER, M. 2005. Environmental regulation of the anaerobic oxidation of methane: a comparison of ANME-I and ANME-II communities. *Environmental Microbiology* **7**, 98–106.

NEUGEBAUER, I., BRAUER, A., DRÄGER, N., DULSKI, P., WULF, S., PLESSEN, B., MINGRAM, J., HERZSCHUH, U. & BRANDE, A. 2012. A Younger Dryas varve chronology from the Rehwiese palaeolake record in NE Germany. *Quaternary Science Reviews* **36**, 91–102.

NIEMANN, H., LÖSEKANN, T., DE BEER, D., ELVERT, M., NADALIG, T., KNITTEL, K., AMANN, R., SAUTER, E. J., SCHLÜTER, M., KLAGES, M., FOUCHER, J. P. & BOETIUS, A. 2006. Novel microbial communities of the Haakon Mosby mud volcano and their role as methane sink. *Nature* **443**, 854–8.

OHFUJI, H. & RICKARD, D. 2005. Experimental syntheses of framboids – a review. *Earth-Science Reviews* **71**, 147–70.

ORANGE, F., CHABIN, A., GORLAS, A., LUCAS-STAAT, S., GESLIN, C., LE ROMANCER, M., PRANGISHVILI, D., FORTERRE, P. & WESTALL, F. 2011. Experimental fossilisation of viruses from extremophilic Archaea. *Biogeosciences* **8**, 1465–75.

ORPHAN, V. J., HOUSE, C. H., HINRICHS, K. U., MCKEEGAN, K. D. & DELONG, E. F. 2001. Methane consuming archaea revealed by directly coupled isotopic and phylogenetic analysis. *Science* **293**(5529), 484–7.

PACTON, M., FIET, N. & GORIN, G. 2006. Revisiting amorphous organic matter in Kimmeridgian laminites: what is the role of the vulcanization process in the amorphization of organic matter? *Terra Nova* **18**, 380–7.

PACTON, M., FIET, N. & GORIN, G. 2007. Bacterial activity and preservation of sedimentary organic matter: the role of exopolymeric substances. *Geomicrobiology Journal* **24**, 571–81.

PACTON, M., FIET, N. & GORIN, G. 2008. Unravelling the origin of ultralaminae in sedimentary organic matter: the contribution of bacteria and photosynthetic organisms. *Journal of Sedimentary Research* **78**, 654–67.

PACTON, M., GORIN, G. & VASCONCELOS, C. 2011. Amorphous organic matter – experimental data on formation and the role of microbes. *Review of Palaeobotany and Palynology* **166**, 253–67.

PACTON, M., WACEY, D., CORINALDESI, C., TANGHERLINI, M., KILBURN, M. R., GORIN, G., DANOVARO, R. & VASCONCELOS, C. 2014. Viruses as new agents of organomineralization in the geological record. *Nature Communications* **5**, 4298.

PAULO, C. & DITTRICH, M. 2013. 2D Raman spectroscopy study of dolomite and cyanobacterial extracellular polymeric substances from Khor Al-Adaid sabkha (Qatar). *Journal of Raman Spectroscopy* **44**, 1563–9.

PENG, X., XU, H., JONES, B., CHEN, S. & ZHOU, H. 2013. Silicified virus-like nanoparticles in an extreme thermal environment: implications for the preservation of viruses in the geological record. *Geobiology* **11**, 511–26.

PIENITZ, R., WALKER, I. R., ZEEB, B. A., SMOL, J. P. & LEAVITT, P. R. 1992. Biomonitoring past salinity changes in an athalassic sub-Arctic lake. *International Journal of Salt Lake Research* **1**, 91–123.

PIRBADIAN, S., BARCHINGER, S. E., LEUNG, K. M., BYUN, H. S., JANGIR, Y., BOUHENNI, R. A., REED, S. B., ROMINE, M. F., SAFFARINI, D. A., SHI, L., GORBY, Y. A., GOLBECK, J. H. & EL-NAGGAR, M. Y. 2014. *Shewanella oneidensis* MR-1 nanowires are outer membrane and periplasmic extensions of the extracellular electron transport components. *Proceedings of the National Academy of Sciences of the United States of America* **111**, 12883–8.

POPA, R., BADESCU, A. & KINKLE, B. K. 2004. Pyrite framboids as biomarkers for iron-sulfur systems. *Geomicrobiology Journal* **21**, 1–14.

PRASAD, V., GARG, R., SINGH, V. & THAKUR, B. 2007. Organic matter distribution pattern in Arabian Sea: Palynofacies analysis from the surface sediments off Karwar coast (west coast of India). *Indian Journal of Marine Sciences* **36**, 399–406.

REGUERA, G., MCCARTHY, K. D., METHA, T., NICOLL, J. S., TUOMINEN, M. T. & LOVLEY, D. R. 2005. Extracellular electron transfer via microbial nanowires. *Nature* **435**, 1098–101.

ROBERTS, J. A., BENNETT, P. C., GONZALEZ, L. A., MACPHERSON, G. L. & MILLIKEN, K. L. 2004. Microbial precipitation of dolomite in methanogenic groundwater. *Geology* **32**(4), 277–80.

SANCHEZ-NAVAS, A., MARTÌN-ALGARRA, A., RIVADENEYRA, M. A., MELCHOR, S., MARTÌN-RAMOS, J. D. 2009. Crystal-growth behaviour in Ca–Mg carbonate bacterial spherulites. *Crystal Growth and Design* **9**, 2690–9.

SANCHEZ-ROMAN, M., VASCONCELOS, C., SCHMID, T., DITTRICH, M., MCKENZIE, J. A., ZENOBI, R. & RIVADENEYRA, M. A. 2008. Aerobic microbial dolomite at the nanometer scale: implications for the geologic record. *Geology* **36**, 879–82.

SASSEN, R., ROBERTS, H. H., CARNEY, R., MILKOV, A. V., DEFREITAS, D. A., LANOIL, B. & ZHANG, C. 2004. Free hydrocarbon gas, gas hydrate, and authigenic minerals in chemosynthetic communities of the northern Gulf of Mexico continental slope: relation to microbial processes. *Chemical Geology* **205**(3–4), 195–217.

SAWLOWICZ, Z. 2000. *Framboids: from their Origin to Application*. Poland: Prace Mineralogiczne, 88 pp.

SCHINK, B. 2002. Synergistic interactions in the microbial world. *Antonie Van Leeuwenhoek* **81**, 257–61.

SCHUBERT, C. J., VAZQUEZ, F., LÖSEKANN-BEHRENS, T., KNITTEL, K., TONOLLA, M. & BOETIUS, A. 2011. Evidence for anaerobic oxidation of methane in sediments of a freshwater system (Lago di Cadagno). *FEMS Microbiology Ecology* **76**, 26–38.

SHINN, E. A., STEINEN, R. P., LIDZ, B. H. & SWART, P. K. 1989. Whitings, a sedimentologic dilemma. *Journal of Sedimentary Petrology* **59**, 147–61.

SMOL, J. 1988. Chrysophycean microfossils in paleolimnological studies. *Palaeogeography, Palaeoclimatology, Palaeoecology* **62**, 287–97.

SONDI, I. & JURACIC, M. 2010. Whiting events and the formation of aragonite in Mediterranean Karstic Marine Lakes: new evidence on its biologically induced inorganic origin. *Sedimentology* **57**, 85–95.

SORREL, P., OBERHÄNSLI, H., BOROFFKA, N. G. O., NOURGALIEV, D., DULSKI, P. & RÖHL, U. 2007. Control of wind strength and frequency in the Aral Sea basin during the late Holocene. *Quaternary Research* **67**, 371–82.

SPADAFORA, A., PERRI, E., MCKENZIE, J. A. & VASCONCELOS, C. 2010. Microbial biomineralization processes forming modern Ca:Mg carbonate stromatolites. *Sedimentology* **57**, 27–40.

STAMS, A. J. M. & PLUGGE, C. M. 2009. Electron transfer in syntrophic communities of anaerobic bacteria and archaea. *Nature Reviews Microbiology* **7**, 568–77.

SUTTLE, C. A. 2007. Marine viruses – major players in the global ecosystem. *Nature Reviews in Microbiology* **5**, 801–12.

SWIERCZYNSKI, T., LAUTERBACH, S., DULSKI, P., DELGADO, J., MERZ, B. & BRAUER, A. 2013. Mid- to late Holocene flood frequency changes in the northeastern Alps as recorded in varved sediments of Lake Mondsee (Upper Austria). *Quaternary Science Reviews* **80**, 78–90.

TALBOT, M. R. & KELTS, K. 1986. Primary and diagenetic carbonates in the anoxic sediments of Lake Bosumtwi, Ghana. *Geology* **14**, 912–6.

THAUER, R. K. & SHIMA, S. 2008. Methane as fuel for anaerobic organisms. *Annals of the NY Academy of Sciences* **1125**, 158–70.

TURCQ, B., ALBUQUERQUE, A. L. S., CORDEIRO, R. C., SIFEDDINE, A., SIMOES FILHO, F. F. L., SOUZA, A. G., ABRÃO, J. J., OLIVEIRA, F. B. L., SILVA, A. O. & CAPITÂNEO, J. 2002. Accumulation of organic carbon in five Brazilian lakes during the Holocene. *Sedimentary Geology* **148**, 319–42.

VALENTINE, D. L. & REEBURGH, W. S. 2000. New perspectives on anaerobic methane oxidation. *Environmental Microbiology* **2**, 477–84.

VASCONCELOS, C. & MCKENZIE, J. A. 1997. Microbial mediation of modern dolomite precipitation and diagenesis under anoxic conditions (Lagoa Vermelha, Rio de Janeiro, Brazil). *Journal of Sedimentary Research* **67**, 378–90.

VASCONCELOS, C., MCKENZIE, J. A., BERNASCONI, S., GRUJIC, D. & TIENS, A. J. 1995. Microbial mediation as a possible mechanism for natural dolomite formation at low temperatures. *Nature* **377**, 220–2.

VIGNERON, A., CRUAUD, P., PIGNET, P., CAPRAIS, J. C., GAYET, N., CAMBON-BONAVITA, M. A., GODFROY, A. & TOFFIN, L. 2013. Bacterial communities and syntrophic associations involved in anaerobic oxidation of methane process of the Sonora Margin cold seeps, Guaymas Basin. *Environmental Microbiology*, published online 13 December 2013. doi: 10.1111/1462–2920.12324.

VINCENT, W. F., WHYTE, L. G., LOVEJOY, C., GREER, C. W., LAURION, I., SUTTLE, C. A., CORBEIL, J. & MUELLER, D. R. 2009. Arctic microbial ecosystems and impacts of extreme warming during the International Polar Year. *Polar Science* **3**, 171–80.

VUILLEMIN, A., ARIZTEGUI, D., DE CONINCK, A. S., LÜCKE, A., MAYR, C., SCHUBERT, C. J. & The Pasado Scientific Team. 2013. Origin and significance of diagenetic concretions in sediments of Laguna Potrok Aike, southern Argentina. *Journal of Paleolimnology* **50**, 275–91.

WALDRON, S., HALL, A. J. & FALLICK, A. E. 1999. Enigmatic stable isotope dynamics of deep peat methane. *Global Biogeochemical Cycles* **13**(1), 93–100.

WARREN, J. 2000. Dolomite: occurrence, evolution and economically important associations. *Earth-Science Reviews* **52**, 1–81.

WARTHMANN, R., LITH, Y. V., VASCONCELOS, C., MCKENZIE, J. A. & KARPOFF, A. M. 2000. Bacterially induced dolomite precipitation in anoxic culture experiments. *Geology* **28**, 1091–4.

WILHELM, S. W. & SUTTLE, C. A. 1999. Viruses and nutrient cycles in the sea. *Bioscience* **49**, 781–8.

WILKIN, R. T. & BARNES, H. L. 1997. Formation processes of framboidal pyrite. *Geochimica et Cosmochimica Acta* **61**, 323–39.

WILKEN, L. R., KRISTIANSEN, J. & JÜRGENSEN, T. 1995. Silica-scaled chrysophytes from the peninsula of Nuusuaq/Nûugssuaq. *Nova Hedwigia* **61**, 355–66.

WILKINSON, A. N., HALL, R. I. & SMOL, J. P. 1999. Chrysophyte cysts as paleolimnological indicators of environmental change due to cottage development and acidic deposition in the Muskoka-Haliburton region, Ontario, Canada. *Journal of Paleolimnology* **22**, 17–39.

WRIGHT, D. 1999. The role of sulphate-reducing bacteria and cyanobacteria in dolomite formation in distal ephemeral lakes of the Coorong region, South Australia. *Sedimentary Geology* **126**, 147–57.

WRIGHT, D. T. & OREN, A. 2005. Non-photosynthetic bacteria and the formation of carbonates and evaporites through time. *Geomicrobiology Journal* **22**, 27–53.

WRIGHT, D. T. & WACEY, D. 2005. Precipitation of dolomite using sulphate-reducing bacteria from the Coorong Region, South Australia: significance and implications. *Sedimentology* **52**, 987–1008.

YAU, S., LAURO, F. M., DEMAERE, M. Z., BROWN, M. V., THOMAS, T., RAFTERY, M. J., ANDREWS-PFANNKOCH, C., LEWIS, M., HOFFMAN, J. M., GIBSON, J. A. & CAVICCHIOLI, R. 2011. Virophage control of antarctic algal host–virus dynamics. *PNAS* **108**, 6163–8.

ZEEB, B. A., CHRISTIE, C. E., SMOL, J. P., FINDLAY, D., KLING, H. & BIRKS, H. J. B. 1994. Responses of diatom and chrysophyte assemblages in Lake 227 to experimental eutrophication. *Canadian Journal of Fisheries and Aquatic Sciences* **51**, 2300–11.

ZEEB, B. A., DUFF, K. E. & SMOL, J. P. 1990. Morphological descriptions and stratigraphic profiles of chrysophycean stomatocysts from the recent sediments of Little Round Lake, Ontario. *Nova Hedwigia* **51**, 361–80.

ZEEB, B. A. & SMOL, J. P. 1993. Postglacial chrysophycean cyst record from Elk Lake, Minnesota. In *Elk Lake, Minnesota: Evidence for Rapid Climate Change in the North-Central United States, Geological Society of America Special Paper 276* (eds J. P. Bradbury & W. E. Dean), pp. 239–49. Boulder, Colorado: Geological Society of America.

ZEEB, B. A. & SMOL, J. P. 1995. A weighted-averaging regression and calibration model for inferring lakewater salinity using chrysophycean cysts from lakes in western Canada. *International Journal of Salt Lake Research* **4**, 1–23.

https://doi.org/10.1017/S0016756814000831 Published online by Cambridge University Press